UNIVERSITY OF TURKU

Activated phosphodiesters as model compounds for RNA cleavage

Department of Chemistry
Faculty of Science
Master's thesis

Author:
Jasmin Koski

7.5.2024
Turku

Master's thesis

Subject: Bio-organic Chemistry, Chemistry of Drug Development
Author: Jasmin Koski
Title: Activated phosphodiester as model compounds for RNA cleavage
Supervisor: Satu Mikkola
Number of pages: 51 pages
Date: 7.5.2024

Phosphodiester bond cleavage reaction has gained significant attention for potential biotechnological and pharmacological applications. Phosphodiester bonds are prevalent structures found in both DNA and RNA, while phosphate esters are also found in carbohydrates and their conjugates. Recent studies have focused on using RNA model compounds to develop artificial nucleases, aiming to replicate the catalytic efficiency of natural enzymes. Among these models, one 2-hydroxypropyl phosphate model compound, HPNP, has been widely used since it has offered a simplified approach despite its structural differences from natural occurring RNA.

This study explores three RNA model compounds, HPNP and its analogues HPHP and HPCP, with the aid of kinetic methods to expose their individual features regarding phosphodiester cleavage reaction. The results provide comparable data to naturally occurring RNA transesterification reaction and help to assess the suitability of the compounds. Experimental methodologies reflect transition state theory, with results based on calculations acquired from a modified Eyring equation.

Kinetic measurements were divided into two reaction phases for the model compounds, exploring their reactivity at different temperatures and pH levels. Samples were withdrawn from each reaction solution in suitable intervals and analyzed with RP-HPLC. The collected HPLC-data was further analyzed to comprehend reaction kinetics and the mechanism behind the transesterification reactions. Unlike some previous studies on similar small model compounds, which have shown isomerization affecting reactivity, HPNP and its analogues showed no such variation.

HPNP demonstrated faster reaction rates due to its superior leaving group character compared to HPCP and HPHP. The pH-rate profiles exhibited minimal variations between compounds, resembling previously reported research data obtained with similar small molecular models. Calculated moderately negative β_{LG} values suggested the nucleophilic attack being the rate limiting step of the reaction. The activation parameters indicated positive enthalpy ($\Delta H^{\neq}$) and negative entropy ($\Delta S^{\neq}$) of activation in variable levels for each model compound, with lowered activation energy barriers in acid catalyzed reactions.

This study offers unique insight into the phosphodiester cleavage reaction of RNA model compounds, while deepening out understanding of 2-hydroxypropyl phosphates' reactivity. The results support previous findings regarding the potential of 2-hydroxypropyl phosphates as artificial nucleases, despite their structural differences from natural RNA characteristics concerning nucleophiles and leaving groups. The findings of this study contribute to the ongoing development of RNA model compounds for biotechnological and pharmacological purposes. The results of this study on 2-hydroxypropyl phosphates of HPHP, HPCP and HPNP represent the first full kinetic analysis reported to date.

Key words: Phosphodiester bond cleavage, RNA model compounds, Kinetic methods, Transesterification reaction, 2-hydroxypropyl phosphates

Table of contents

ABBREVIATIONS

ASO	Antisense Oligonucleotide
BNPP	bis-(p-nitrophenyl) phosphate
CRISPR-Cas	Clustered Regularly Interspaced Short Palindormic Repeats-CRISPR-associated
DNA	Deoxyribonucleic Acid
HPCP	2-chlorophenyl-2-hydroxypropyl phosphate
HPHP	2-hydroxypropyl phenyl phosphate
HPNP	2-hydroxypropyl-4-nitrophenyl phosphate
mRNA	Messenger Ribonucleic Acid
MMP	Methyl Phosphate Dianion
MS	Mass Spectrometry
ncRNA	Non-coding Ribonucleic Acid
NMR	Nuclear Magnetic Resonance
RP-HPLC	Reversed-Phase High-Performance Liquid Chromatography
ROS	Reactive Oxygen Species
RNA	Ribonucleic Acid
rRNA	Ribosomal Ribonucleic Acid
siRNA	Small Interfering Ribonucleic Acid
snRNA	Small Nuclear Ribonucleic Acid
tacn	Triazacyclononane
tRNA	Transfer Ribonucleic Acid
UPCP	Uridine-3'-(2-Chlorophenyl)-Phosphate
UMP	Uridine-monophosphate
UpU	Uridylyl-(3',5')-Uridine

1 Introduction

1.1 Unlocking transesterification: Artificial RNA Models for Drug Development

RNA therapeutics are transforming the traditional drug approaches by exploiting the unique properties of RNA molecules, thus expanding therapeutic targets for disease diagnosis, prevention, and treatment (1). Currently, small molecular and protein or antibody -based compounds rule the pharmaceutical market and are the most studied for drug development purposes. However, the traditional medicinal development has entered a new chapter as the mysteries of complex biological physicochemical characteristics have begun to unravel (2).

RNA's ability to both manipulate and encode the genetic information of living organisms, makes it a remarkable macromolecule and a highly potential candidate for biotechnology and biopharmaceutical applications (3). Modern innovations offer novel strategies to combat infectious diseases, cancer, metabolic disorders, neurodegenerative conditions, and rare genetic diseases, many of which previously lacked effective treatment or were completely untreatable (2; 4). The potential of RNA lies in high specificity and a broad spectrum of targets, including proteins, transcripts, and genes, often inaccessible to small molecular drugs (4).

RNA's potential extends to the transcriptome, where mRNA can be translated into proteins and functional ncRNAs, and to genome editing through methods such as CRISPR-Cas. Various RNA-based therapeutics, including aptamers, antisense oligonucleotides (ASO), and siRNA, are already in clinical use. Innovations such as the mRNA vaccine for COVID-19 pandemic demonstrates the efficacy of these approaches in replacement therapies and vaccination strategies (2; 5). Nevertheless, many challenges must be overcome in the drug development process before RNA-based therapeutics can overpower the current gold standard of medicinal therapeutics (5).

Obstacles related to RNA therapeutics include issues with intracellular delivery, immune-related toxicity, and poor pharmacological properties. Additionally, challenges such as identifying novel RNA therapeutical entities and viable RNA targets are being faced (5; 6). The mechanisms of action of emerging therapeutical agents are based on their ability to modify RNA's functionality (1). Artificially developed RNA model compounds provide insight to some of the challenges mentioned and offer an alternative approach to observe the physicochemical properties. These features focus to reveal fine nuances of chemical structure

and reactivity, which can be directly or indirectly proportional for drug development purposes (7). Studies conducted with small molecular models, such as the activated phosphodiester models, provide additional information in relation to reactions of naturally occurring nucleic acids (8).

1.2 The structure and functions of naturally occurring nucleic acids

1.2.1 Basic Structure of Nucleic Acids – DNA and RNA

Nucleic acids can be divided into two main types, DNA (deoxyribonucleic acid) and RNA (ribonucleic acid). Both are composed of similar building blocks but differ in their location, structure, and functionalities. They are the primary information-carrying molecules, responsible for the storage and expression of genetic information (9). Nucleic acid chains (Figure 1.) are formed through the polymerization process of nucleotides. The individual nucleotides consist of three main components: of a nitrogenous base, an aldopentose sugar and one or more phosphate groups (10; 11).

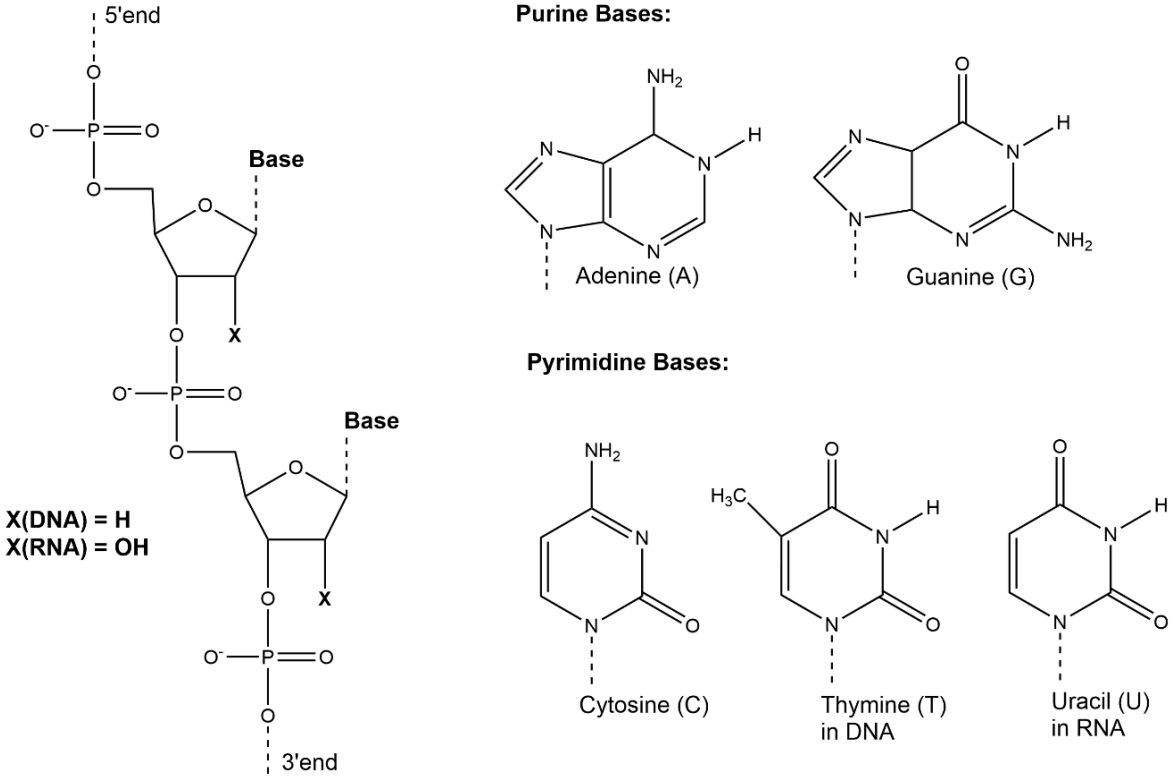

Figure 1. Basic chain structure of nucleic acids (DNA and RNA). The figure is drawn as shown in reference (10).

The first main component, the nitrogenous bases, also known as the nucleobases, consists of heterocyclic aromatic ring structures of either pyrimidine, or purine origin. The latter consists

of a double ring structure formed from the fusion of a pyrimidine ring to an imidazole ring. The nucleobases are further divided into two groups based on their ring structure. The monocyclic pyrimidine bases are thymine (T), cytosine (C) and uracil (U), bicyclic purine bases are adenine (A) and guanine (G) (10; 11). A glycosidic bond links the sugar to the nucleotide, with pyrimidine bases connecting to the sugar moiety via C1'-N1 -bond and purine bases via C1'-N9 -bond (12).

The second structural element of nucleotides is the aldopentose sugar. In RNA, D-ribose forms the sugar structure, with a hydroxyl group attached to the 2'-position of the pentose sugar (10). The sugar structure in DNA, D-2-deoxyribose, differs from that in RNA, with a hydrogen atom at the 2'-position instead of the hydroxyl group (12).

The third main component of nucleotides is the phosphate group, which forms a covalent bond between sugar units of adjacent nucleotides (12) This phosphodiester link is established by the phosphate between two nucleotide sugar structures, where the hydroxyl group at the C5'-position of the first nucleotide sugar links to the hydroxyl group at the C3'-position of the second nucleotides sugar (10; 11). RNA's phosphodiester bonds are less stable than in DNA, enabling RNA molecules to be more flexible to changes in environmental conditions, such as heat and pH (13).

As the phosphate and sugar portions of the nucleotides polymerize, they form a chain structure, which acts as a firm structural backbone to the RNA and DNA molecules (12). The nucleobases extend from this main backbone structure, interacting complementarily between two nucleotide chains via hydrogen bonding (Figure 2.). These interacting nucleobases represent the basic units of genetic code, in which the biological function is dependent on their order and pairing (10).

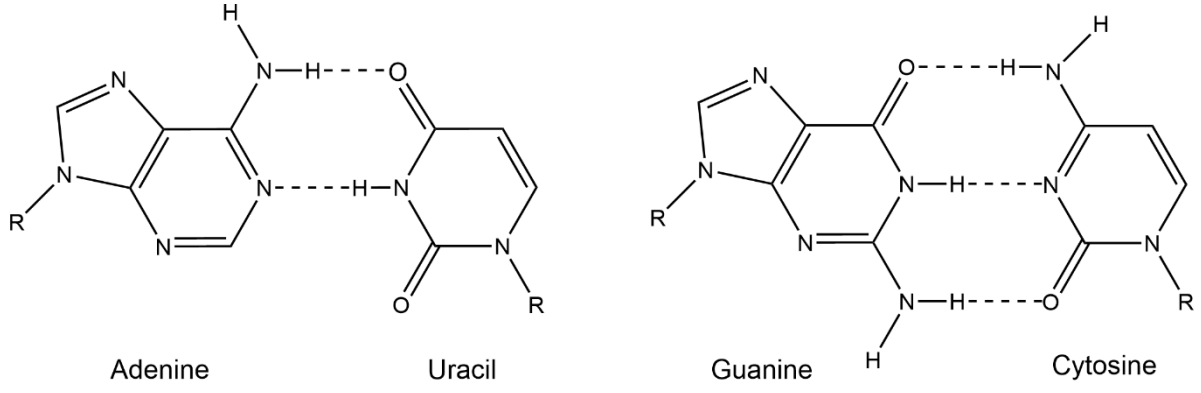

Figure 2. Hydrogen bonding in RNA.

Watson-Crick base-pairing principle determines nucleotides pairing. In DNA, adenine (A) pairs with thymine (T), guanine (G) with cytosine (C). In RNA, thymine bases are replaced by uracil (U), which pairs with adenine (A) (12). The genetic code itself is composed of nucleotides forming codons, sequences of three nucleotides, each correlating to the encoding of a specific amino acid or the termination of protein synthesis (13).

DNA forms a double helical structure, in which the complementary chains of DNA run in opposite, antiparallel directions, with the 5’ carbon of one chain facing the 3' carbon of the other. The exterior of the DNA double helix exhibits specific regions of major and minor grooves, where other molecules, such as polypeptides, can insert themselves (13). RNA does not from a complementary double helical secondary structure like DNA, although the nucleobase pairing occurs in a similar manner (10). Instead, the nucleotides of linear RNA strand interact freely by forming complex and variable secondary structures inside each molecule (14).

The secondary structures of RNA and DNA motifs are progressed into more intricate tertiary and quaternary structures, thus further highlighting the differences in their functionalities (15; 16). Functional structures of RNA are often formed by small structural motifs which are organized three-dimensionally, as self-complementary base pairing interactions occur in different regions of the same RNA chain (14). The higher reactivity of the ribose sugar 2’-OH hydroxyl groups plays an important role in the formation and conformations of RNA molecules, in addition to the Watson-Crick and Hoogsten base pairing geometries. Furthermore, several non-canonical base pairs stabilize the molecular structure of RNA (14; 17).

The secondary structure of RNA manifests in multiple forms, creating structures such as hairpins, loops, and bulges based on the base-pairing principles (14). More complex tertiary structures emerge as longer strands of RNA create more stabilized three-dimensional structures, resembling protein-like configurations. The stabilization of these tertiary structures involves electrostatic interactions and base stacking, among other factors (18).

1.2.2 The main reactions of naturally occurring RNA

The lifecycle of RNA differs significantly from that of DNA, as they serve different purposes in the biological systems, which contribute to the survival and generational development of living organism. DNA stores genetic information within membrane-protected cell organelles,

primarily in the nucleus and mitochondria, while RNA is synthesized and stored in the cytoplasm of each cell (10).

RNA plays more versatile roles in organisms' function and molecular activity compared to DNA, which mainly stores the genetic information and regulates its expression and transmission between generations (10; 13). Many functions of RNA are regulated by proteins, such as the energy converting enzymes. Messenger RNA (mRNA) acts as the intermediary molecule in the process of converting the base sequence, the known order of nucleobases in the DNA chain structure, into a functioning protein (13).

Some RNA transcripts produced are noncoding types of RNA and can have functions of their own. For example, ribosomal RNA (rRNA), the major component of ribosomes, participates in mRNA and ribosome alignment and functions as the catalyst for peptide bond formation between amino acids during protein synthesis. Transfer RNA (tRNA) is responsible for delivering individual amino acids to be used in translation (13). Small nuclear RNA (snRNA) is a crucial component of the spliceosome, a large protein complex required for RNA processing to generate mRNA (19). Regulatory RNA molecules, such as microRNA (miRNA) and small interfering RNA (siRNA) participate in the inhibition of translation or destruction of RNA transcript. Additionally, some RNA molecules can act as enzymes themselves in chemical reactions related to catalytic cleavage and ligation reactions on substrate RNA molecules (13), in addition to the properties mentioned above.

Due to its location in living organisms, RNA is more exposed to the environmental changes and affected by surrounding biochemical cascades and processes. The smaller size of RNA and the lack of corresponding structural protection via intramolecular interactions, as in DNAs structure, make it more fragile (12). RNA also possesses intramolecular nucleophilicity due to the additional OH group in the sugar moiety, thus making RNA structures more prone to reactive species (20).

1.2.3 Oxidative reactions of RNA

Biological reactions can produce metabolic components, or living organisms can be exposed to chemical agents that promote formation of reactive oxygen species (ROS) or free radicals (21). These components can react rapidly with biomacromolecules, such as nucleic acids, and alter their functionalities with dramatic consequences for the living organism. Some free radicals are part of the normal cell cycle while others occur spontaneously, causing unwanted long-term

effects on the living organism (22). Free radicals are highly reactive, as the unpaired electrons within them tend to react rapidly. Biologically important free radicals are oxygen-derived, in which hydroxyl radicals, in particular, cause most of the damage to coding and noncoding RNA (21).

Since RNA lacks the same ability as DNA to protect and correct the effects of oxidative reactions, damage to its structure can lead to severe outcomes such as premature cellular aging, dysfunctional cell metabolism, and even cellular death (21). High concentrations of oxidative RNA have been linked in humans to multiple diseases such as neurogenerative diseases, diabetes, atherosclerosis, and schizophrenia (23). Oxidative reactions involve alterations to the base or sugar moieties of RNA, and reactions solely derived from hydroxyl radicals are known to cause over 20 types of radical-induced modifications to base moieties. (24).

1.2.4 Transesterification of RNA

RNA's transesterification reaction is involved in many different types of coding and noncoding RNA systems (25; 8). The structural uniqueness of RNA involves the 2'-hydroxyl group's ability to function as an intramolecular nucleophile (25). The phosphodiester bond in the RNA backbone is broken as the sugar-phosphate bond breaks and cleaves the RNA molecule (10). The adjacent 2'OH group of the ribose sugar attacks the phosphate of the phosphodiester bond, forming a pentacoordinate intermediate structure that leads to the cleavage of the 5'-linked bond (Figure 3). The reaction proceeds to produce 2',3'-cyclic phosphate, which produces a mixture of 2'- and 3'-terminal phosphate groups upon hydrolysis (25; 26).

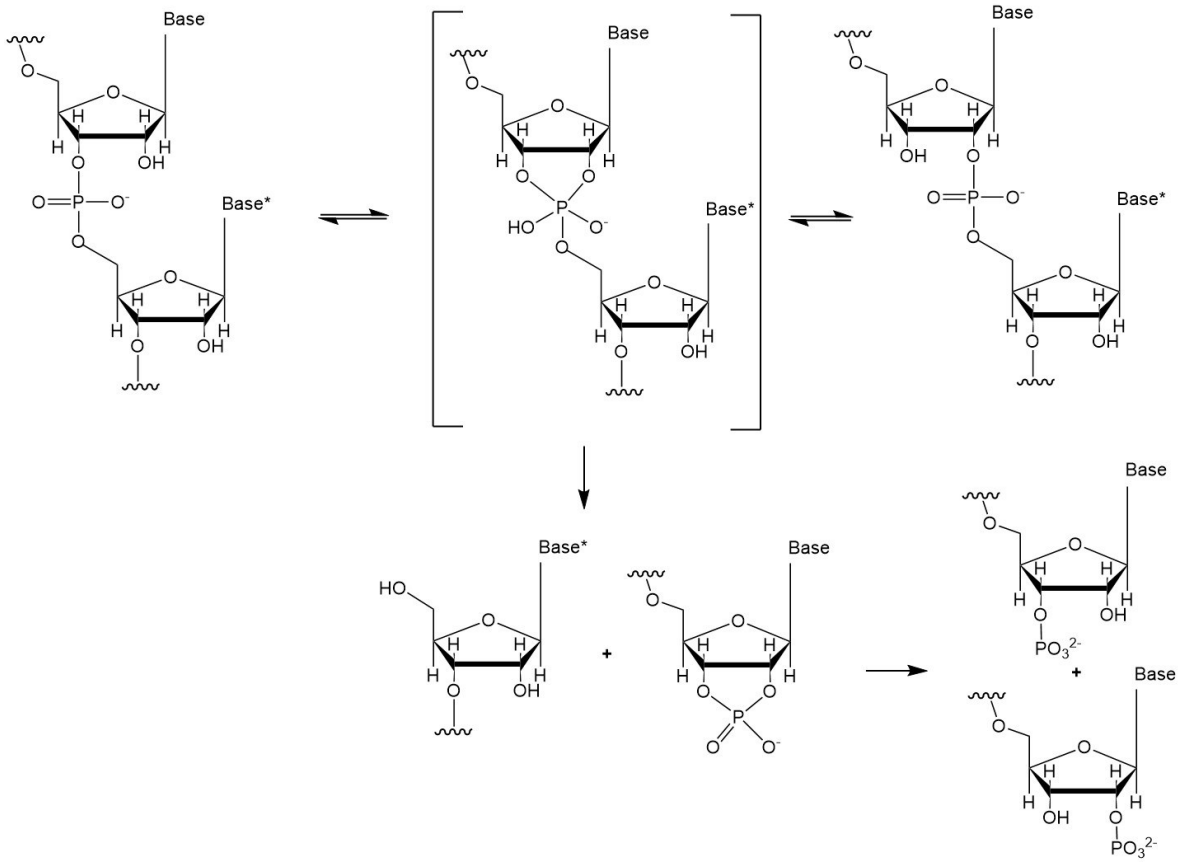

Figure 3. RNA transesterification under neutral conditions, resulting in phosphodiester bond cleavage or isomerization of phosphorane intermediate. The figure is drawn based on the reference (25).

The isomerization of naturally occurring RNA occurs through the three-dimensional re-orientation of the intermediate structure. The resulting 2',5'-phosphodiester bond forms as the ligands undergo apical and equatorial re-positioning (25).

The hydroxyl groups apical position facilitates the formation of the intermediate structure, a process guided by the principles of Westheimer's rules, which dictate the nucleophile's behavior within the reaction. The phenomenon is influenced by the three-dimensional positioning of ligands in the pentacoordinate structure and their electronegativity (27). Respectively, electropositive ligands prefer the equatorial position, while electronegative ligands in return prefer the apical position of trigonal bipyramidal pentacoordinate compounds (28).

The transesterification reaction is dependent on the reaction conditions, such as the pH, and can occur spontaneously or with the aid of a catalyst or enzymes, known as nucleases (8). Transesterification via phosphorane intermediate involves hydroxide ion catalysis in neutral and basic conditions as the primary mechanism for naturally occurring RNA.

The leaving group is identified as an alkoxy group, as indicated by the β_{LG} -value of –1.28 (29). The single-stranded RNA transesterification reaction can emerge spontaneously through self-cleavage in basic solutions, in which the circulating free hydroxide ions deprotonate the 2'OH of the RNA's ribose sugar. The possibility of a spontaneous cleavage of RNA decreases as the structure becomes more complex and thus more stabilized. The cleavage of secondary structures can involve enzymes in addition to spontaneous cleavage (25).

One of the main strategies related to RNA as therapeutic agent involves its ability to modulate its function through phosphodiester bond cleavage reactions (8). In this context, it becomes essential to thoroughly understand RNA's reactivity, including a profound comprehension of the precise reaction mechanism and features that can expedite transesterification (30).

However, the highly complex reactivity of RNA in its natural environment makes it a challenging structure to study since the reactions are difficult to replicate and mimic in vitro (31). The challenges of obtaining accurate data of naturally occurring RNA reactions have been able to overcome with the aid of artificial RNA model compounds; thus, continuous research is required to achieve a comprehensive analysis on their reactivity (8).

1.3 Studies on the phosphodiester cleavage with small molecular models

1.3.1 Experimental methods

The transesterification reaction of RNA can be investigated using artificially developed RNA model compounds, which resemble features of naturally occurring RNA. Various theoretical and analytical techniques, as well as experimental approaches, involve combined efforts to truly understand the structure and function of the transesterification reaction (8).

Kinetic experiments provide insight into understanding how different reaction conditions affect the behavior of the studied compounds (7; 32). Enzymatic and chemical cleavage reactions can be studied in various ways with the aid of RNA model compounds, RNA-specific enzymes such as RNases, or chemical agents such as hydroxide ions, to gather information about the structural reaction details (32).

A comprehensive analysis of reaction mechanism can be gathered by well-known kinetic tools such as pH-rate profiles, solvent isotope effects, buffer catalysis, and the effect of structural variations on compounds' reactivity (8). Among these tools, pH rate profile is particularly useful to clarify the mechanisms across a wide pH range. It reveals several features directly

influencing the reaction mechanisms, including the identification of rate-limiting steps, the role of acid-base catalysis, and the influence of pH-dependent pKa values on reaction kinetics (33).

Quantitative measurement tools such as the reaction activation parameters and the leaving group effect, reveal fine nuances of structural details (8). The suitability of a leaving group in a reaction can be evaluated with beta leaving group value (β_{LG}). This value reflects the dependency between the leaving group and the reaction rate. A higher negative β_{LG} value indicates a more favorable leaving group (34).

Spectroscopy techniques, such as Nuclear Magnetic Resonance (NMR) provide insights into the conformation and dynamics of phosphodiester bonds, while infrared (IR) spectroscopy can be exploited to unveil the vibrational modes of the bond (35). X-ray crystallography exploits growing RNA crystals' X-ray diffraction patterns analysis and can be used to investigate the phosphodiester backbone to gather high-resolution details of its three-dimensional structure (36). Computational methods, such as molecular dynamics simulations, offer insight to the dynamics of phosphodiester linkages (37). Mass spectrometry (MS) can be used to determine the molecular masses to identify the presence and integrity of the studied model compounds (38).

Each approach has its benefits and drawbacks. While studies with naturally occurring RNA provide the most accurate data, they can be technically challenging to execute and may not yield fully quantitative results. Conversely, smaller model compounds offer rapid reactions and convenient analysis but may not fully reflect relevant data due to their structural simplicity (39; 8). Experiments with RNA model compounds have helped to elucidate the nature of nucleophiles and leaving groups. However, these features may not always be applied for physiological reaction environments and therefore represent a more theoretical approach (8).

The biological relevance of small molecular models' reactivity can be controversial, as these reactions are difficult to study in vitro and may not fully reflect the complexity of in vivo reactions (40). Despite the challenges, small molecular models remain a strong contender for RNA-related studies (39). Both non-nucleosidic and nucleosidic small molecular RNA models have been extensively studied for decades (8). Various model compounds have been utilized in studies on reactivity, ranging from naturally occurring RNA to synthetic molecules (figure 4.).

The origin of the synthetic RNA model compounds varies, including compounds with nucleosidic origins such as dinucleoside monophosphates (**1**), 3'-alkylphophates (**2**) and 3'-

arylphosphates (**3**), as well as non-nucleosidic compounds such as 2-hydroxypropyl phosphates (**4**) and bis-(p-nitrophenyl) phosphate (BNPP; **5**) (34; 41).

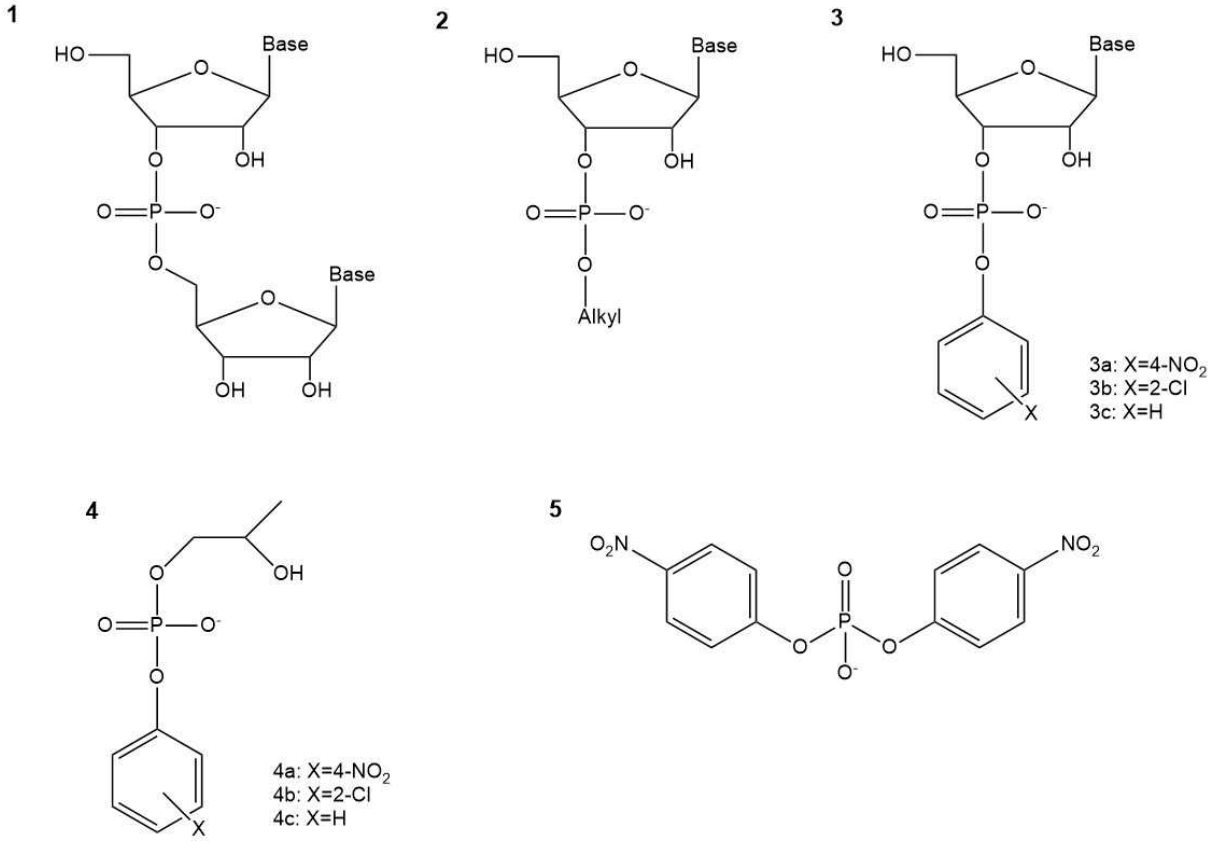

Figure 4. RNA Model Compounds commonly used for reactivity studies. The figure is drawn based on the reference (25).

1.3.2 Insights from Prior Research with nucleoside-based model compounds

As indicated earlier, the reactions of RNA model compounds have been explored with the help of various kinetic tools, such as pH dependence, isotope effects, and structural variations, to unveil their reactivity. Based on these findings, the general characteristics of reaction mechanisms are well established (42). pH dependence and the solvent isotope effects have been studied with both metal-ion complexes and simplified model compounds to reveal more precise allocation of the nucleophilic attack and the leaving group features (8).

Studies with nucleoside -based RNA models have shown that both acids and bases catalyze the cleavage of the phosphodiester bond (41). Analysis of pH rate profiles reveals that the reaction rate is slower in neutral and basic conditions for alkyl esters (43) compared to aryl esters (44). For instance, UPCP, **3b** (45) presents 10^4 higher reactivity compared to 3'5'-UpU (**1**) (46). In

acidic and neutral reaction environments, the phosphodiester cleavage reaction competes with isomerization (47). Despite the presence of competitive reactions of cleavage and isomerization in acidic conditions, the pH rate profiles resemble one another among aryl- and alkyl esters (41).

The properties of different RNA model compounds can also be approached by exploring the leaving group effect in various alkaline or acidic reaction conditions (32). Under acidic conditions, where the leaving group is an alcohol (46), two opposing effects occur: an electronegative group aids nucleophilic attack, but protonation of the leaving group oxygen is hindered due to lower p*K*a (34; 41). The polar nature of the esterified alcohol influences isomerization reactions more than the actual cleavage reaction (34). Studies with nucleoside 3'phosphotriesters have found that symmetric phosphates (43) show a higher β_{LG} value compared to asymmetric (48) 3'phosphotriesters (34).

Uncatalyzed cleavage of neutral phosphodiesters occurs around pH 3, involving nucleophilic attack and concerted proton transfers. pH-independent cleavage of phosphodiester monoanions involves a rare tautomer with a deprotonated 2'-OH function and a neutral phosphate. A moderately negative β_{LG}-value (–0.59) has been reported (49). Isomerization proceeds through the same intermediate. The leaving group's electronegativity affects nucleophilic attack and pseudo-rotation, with more electronegative groups hindering the latter (34).

Base-catalyzed cleavage of nucleoside 3′-phosphodiesters involves nucleophilic attack of a deprotonated 2′-oxy-anion on an anionic phosphate, leading to a dianionic phosphorane intermediate and departure of the leaving group as an alkoxy anion (50). The breakdown of the dianionic phosphorane via the late transition state serves as the rate-limiting step of the reaction leading to cyclic phosphate and the departure of the leaving group as an alkoxy anion. Consistent with this, highly negative β_{LG} values have been observed: according to Kosonen *et al.* (43) base-catalyzed cleavage of 3'-UMP alkyl esters (**2**, B=Uracil) (90°C) yielded a β_{LG} value of –1.10 (±0.05) (43). Cleavage of phosphotriesters exhibits even more negative β_{LG} values than phosphodiesters, in which asymmetric phosphotriesters (48) exhibit lower β_{LG} values than their symmetric counterparts (43).

Conversely, good aryloxy leaving groups result in only moderately negative β_{LG} values. A study by Davis *et al.* (44) determined β_{LG} value of –0.54 (±0,05) for HO^- catalyzed reaction of 3'-UMP aryl esters (**3**, B=Uracil) in bicarbonate buffer (25°C) (44). A similar trend is observed between nucleoside 3′-aryl (51) and 3'-alkyl (52) phosphorothioates, in which the analysis of

leaving group effects reveals a change in the rate-limiting step at a p*K*a of 12.4, indicating that the phosphorane is an intermediate rather than a transition state (34).

The effect of the leaving group can be systematically analyzed using phosphodiesters with different leaving groups, but understanding the impact of the nucleophile is more complex, with only a few studies published. Piccirilli *et al*. (53) synthesized RNA molecules with an extra substituent at C2' position of the ribose to alter the p*K*a of the 2'-OH nucleophiles, resulting in a β_{NUC} value of 0.75 for intramolecular nucleophilic attack in RNA (53; 34). Mancin *et al.* (54; 55) studied the effect of metal-activated nucleophiles on HPNP and BPNP cleavage, determining rate constants as a function of the p*K*a value of the metal-bound H_2O or 2-OH of HPNP. They obtained β_{NUC} values of 0.75 for HPNP and 0.2 for BPNP cleavage (34; 54; 55).

1.3.3 Reactivity of the 2-hydroxypropyl phosphates

HPNP (**4a**) is commonly used as an RNA model compound in both catalyzed and uncatalyzed applications. HPNP (**4a**) obtains a poor nucleophile but good leaving group characteristics. In contrast, naturally occurring RNA (Figure 3) obtains a poor leaving group and good nucleophile, suggesting the departure of the leaving group as the rate-limiting step for RNA cleavage (41). This hypothesis has been demonstrated with Uridylyl-(3',5')-uridine (3',5'-UpU, **1**), obtaining similar features as naturally occurring RNA, possessing a poor leaving group but good nucleophile (56). The high p*K*a-value of 14.4 (56) (90°C) suggest that significant dissociation requires high pH to occur, further implying that pH significantly influences the rate-limiting step of the cleavage reaction (32).

In comparison, the flexible structure of the HPNP (**4a**) hinders the nucleophilic attack compared to the 2'-OH in RNA, whereas the 4-nitrophenol, with a p*K*a of 7.148, functions significantly better as a leaving group than a nucleoside (44). In contrast to 2-hydroxypropyl phosphates (**4**), nucleoside 3'-arylesters (**3**) as RNA model compounds combine both a good nucleophile and a strong leaving group, rendering them more reactive than other RNA models used (50).

The transesterification of 2-hydroxypropyl phosphates follows the same mechanistic steps for spontaneous intramolecular phosphodiester cleavage (Figure 5.), in which the nucleophilic attack has been determined as the rate limiting step. The final steps post phosphorane intermediate formation, result in product formation and departure of the leaving group, with no reported isomerism (41; 57).

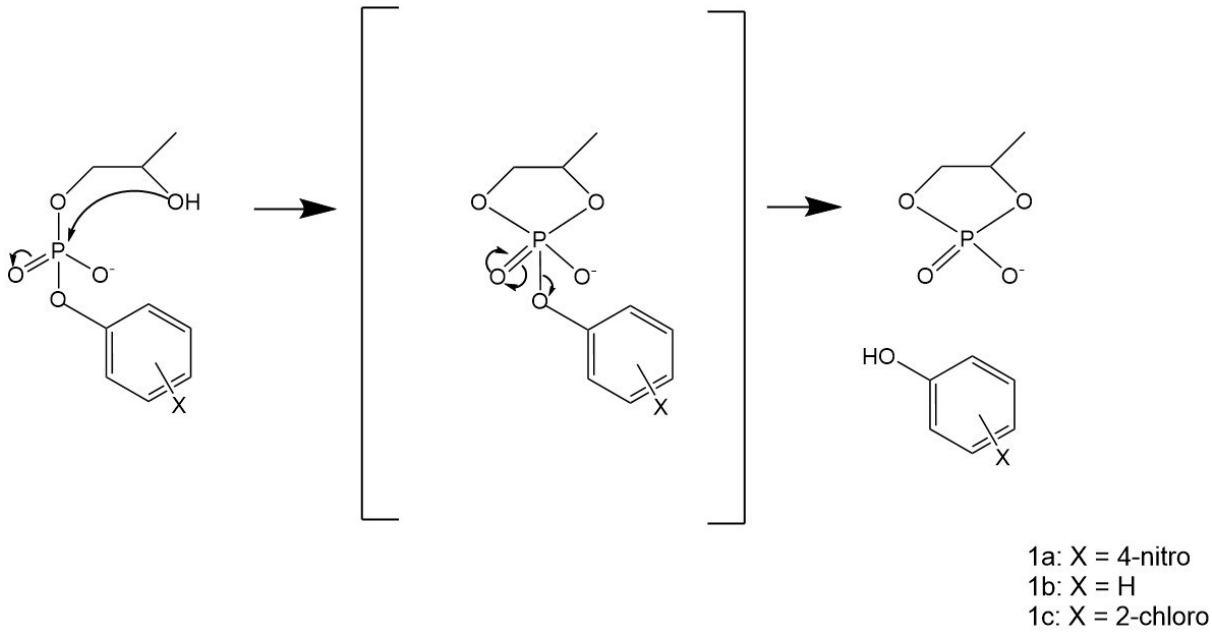

Figure 5. Spontaneous intramolecular transesterification of 2-hydroxypropyl phosphates (1a: HPNP, 1b: HPHP, 1c: HPCP) The figure is drawn based on the reference (57).

Despite numerous studies on various RNA model compounds, the combined effects of nucleophile and the leaving group in 2-hydroxypropyl phosphates have not been determined before, even though 2-hydroxypropyl phosphates such as the HPNP (**4a**) are readily accessible and very popular model compounds (8). 2-hydroxypropyl phosphates have their limited structural mimicry as they do not necessarily directly reflect the structure of RNA molecules and differ in complexity, including functional groups, nucleophile, leaving group character and the diversity of tertiary interactions present in the cellular environment (41).

Studies with HPHP and other phosphodiesters as model compounds for metal ion promoted cleavage have gained a lot of interest for artificial nuclease development (39). Compounds such as BNPP (**5**), HPNP (**4a**), nucleoside 3'-arylesters (**3**) and 3'-alkylesters (**2**) have determined the dependency of phosphodiester bond cleavage on metal complexes of nitrogen ligands as catalysts (39). Metal ion studies with Zn^{2+} and Cu^{2+} complexes have been found particularly suitable because these metal ions are commonly found in the environments in which naturally occurring RNA operates (8; 39).

No universal mechanism for metal ion promoted cleavage has been found despite the efforts (39). The catalysis mechanism of the cleavage suggests various propositions from electrophilic and nucleophilic catalysis to general acid-base catalysis, depending on the studied RNA model compound and the possible mono- or bimetallic nature of the catalyst (8).

Metal catalysts exhibit diverse mechanisms based on the model compound and its individual structural characteristics. For instance, research by Tjioe *et al.* (58) compared mononuclear copper (II)–tacn complexes to three bis(1,4,7-triazacyclononane) binuclear copper (II) complex ligands in their ability to accelerate BNPP (**5**) and HPNP (**4a**) phosphodiester cleavage. At pH 7, binuclear copper (II) complexes increased BNPP (**5**) cleavage rates by 4–18 times compared to the mononuclear copper complex. Similar phenomena were discovered at pH 6 for HPNP (**4a**) cleavage, which was accelerated by 5–130 times (58).

1.3.3 The objective of the present study

As described in the previous sections, HPNP has been frequently used as an RNA model compound. However, mechanistic studies reveal significant distinctions in both reactivity and reaction mechanisms between HPNP and nucleoside-based model compounds. This study approaches the transesterification reaction of the phosphodiester bond through reaction kinetics by exploring three synthetically prepared activated RNA model compounds. The full kinetic analysis of the three 2-hydoxypropyl phosphates assesses the overall suitability of the compounds as well as the reaction kinetics in comparison to the transesterification reaction of naturally occurring RNA.

In addition, this study sheds light on the complexity of RNA model compound development by exposing the activated 2-hydroxypropyl phosphates reactivity under various reaction temperatures and pH levels across the pH range. The newly gained data on the kinetic features of the studied model compounds ultimately assist the grand scheme efforts to comprehend biological processes related to RNA's functionality. These implications may provide novel insights not only into the field of basic scientific research but also into drug development purposes on a larger scale, particularly related to the reactivity of phosphodiester bonds.

2 Experimental

2.1 Kinetic measurements

RNA model compounds were synthetized in a previous project according to procedure reported in ref. 59 and characterized by spectroscopic analysis before storage. The synthetized RNA model compounds were stored frozen (- 20 °C, in powder form), and their purity was confirmed by HPLC analysis before the experiments were conducted. The kinetic measurements of the three RNA model compounds, HPHP (**4c**), HPCP (**4b**) and HPNP (**4a**), were divided into two reaction phases.

Table 1. Reaction solution composition in different pH-levels

pH	Reaction solution composition
1	0,1 M HCl
2	10 mM HCl, 0,09M NaCl
3	0,1M HCOOH, 0,015M NaOH, 0,085M NaCl
4	0,1M HCOOH, 0,065M NaOH, 0,035M NaCl
5	0,1M CH_3COOH, 0,065M NaOH, 0,035M NaCl
6	0,1M MOBS, 0,013M NaOH, 0,087M NaCl
7	0,1M MOBS, 0,06M NaOH, 0,04M NaCl
8	0,1M CHES, 0,038M NaOH, 0,062M NaCl
9	0,1M CHES, 0,087M NaOH, 0,013M NaCl
10	0,025M K_2HPO_4, 0,005M NaOH, 10,5mM NaCl
11	0,025M K_2HPO_4, 0,0175M NaOH
12	10 mM NaOH, 0,09 M NaCl
13	0,1 M NaOH

In the phase one experiments, reactions were conducted at controlled temperatures of 25, 50, 75, and 90 °C using reaction solutions (Table 1.) with high- and low-end pH-values. Phase one experiment reactions were conducted for HPHP (**4c**) and HPCP (**4b**) model compounds at pH-levels 1 and 13, while for the HPNP (**4a**) model compound, reactions were conducted at pH-levels 1 and 10.

Phase two of the experiments involved reactivity studies for each model compound at various pH-levels, conducted at a controlled temperature of 90 °C. The pH-scale ranged from 1 to 13 for the HPHP (**4c**) and HPCP (**4b**) reactions, and from 1 to 10 for the HPNP(**4a**) reactions.

The ionic concentration for pH-levels between 2 and 12 was adjusted with 1,0 M NaCl accordingly. The p*K*a-values of pH-levels 3 to 11 were adjusted with 1,0 M NaOH based on literature p*K*a-values (Table 2.) to maintain the desired buffer ratio at higher reaction temperatures.

Table 2. Buffered reaction solutions' p*K*a-values

Compound	**Formula**	**p*K*a (90°C)**
Formic Acid	HCOOH	3.75 (60)
Acetic Acid	CH_3COOH	4.75 (60)
4-(morpholin-4-yl) butane-1-sulfonic acid (MOBS)	$C_8H_{17}NO_4S$	6.82 (61)
2-(Cyclohexylamino)ethane sulfonic acid (CHES)	$C_8H_{17}NO_3S$	8.2 (62)
Dipotassium hydrogen phosphate	K_2HPO_4	10.64 (60)

Samples were withdrawn at suitable intervals and either kept in an ice bath or frozen and thawed to room temperature prior to HPLC analysis. The peak magnitude changes observed during the HPLC analysis, including the depletion of the start material peak and the increase of the product material peak, indicated successful progression of the reaction.

Individual test reaction in phase one and phase two experiments were monitored until at least the first half-life was reached, at which point the starting material had depleted to at least half of its original amount.

The HPLC analysis data were recorded onto corresponding test sheet (Appendix 1. Pre-filled test sheet example) and plotted using the Origin statistical program. A full kinetic analysis was completed based on the data accumulated from both phase one and two experiments. The following discussion will explain in more detail the steps involved in the kinetic measurements, including phases one and two, as well as the HPLC analysis.

2.1.1 Phase one experiments

Phase one experiments gathered information of each RNA model compound's general reaction profile in different temperature and pH-level reaction environments. The phase one reaction

series were initiated by testing the reactivity first in extreme alkaline reaction solutions, for the HPHP (**4c**) and HPCP (**4b**) at pH-level 13 (0,1 M NaOH), and for HPNP (**4a**) at pH-level 10 (0,025M K_2HPO_4, 0,005M NaOH, 10,5mM NaCl). Experiments were performed individually to minimize human error related to pipetting frequency and data recording.

2,5 ml of reaction solution was added to a sealed glass tube and transferred into a preheated 90 °C thermostatic water or oil-water bath for incubation. Small microcentrifuge tubes were prelabelled with a running test number sequence and a running sample number and placed on an ice bath. To stop the reaction from proceeding post sample collection, 15 µl of 1% acetic acid was added to each microcentrifuge tube prior to sample collection.

A primary solution was prepared by adding a small amount of the model compound (powder) to 0,5 ml of ultra-purified water (H_2O MilliQ). Prior to initiating experiments, the potency of the primary solution was confirmed by HPLC analysis, in which the magnitude of the start material peak was ensured to be large enough for sufficient reaction monitoring. 10-50 µl of the corresponding model compound's primary solution was added to the preheated reaction solution tube and mixed vigorously. The addition of the primary solution to the reaction tube initiated reaction timing, and the first initial baseline sample was taken immediately after mixing. Sample aliquots of 100-150 µl were withdrawn from the incubating reaction tube at varying frequencies and transferred into the prelabelled microcentrifuge tubes on ice bath upon sample aliquoting.

Same optimized reaction conditions, sample, and reaction solution amounts were used for the remaining reaction series at temperatures of 75, 50 and 25 °C. The frequency of sample aliquoting was prolonged as the temperature decreased. The phase one reaction series were repeated in an acidic reaction solution of pH 1 for each model compound using the same optimized methods, apart from adding acetic acid to microcentrifuge tubes.

2.1.2 Phase two experiments

Phase two experiments gathered information of each RNA model compounds reactivity on a wider pH-scale to form a pH-profile for each model compound tested based on experimentally determined reaction rate constants (*k*). The reaction solutions (Table 1.) used for the experiments were in between pH 1 to 13 for HPHP (**4c**) and HPCP (**4b**) model compounds, and in between pH 1 to 10 for the HPNP (**4a**).

The reaction temperature was set to 90 °C for all phase two experiments. Phase two experiments were conducted for each pH-level by using the same optimized reaction conditions, sample, and reaction solution amounts as in the phase one experiments. To stop reactions from proceeding post sample collection, 10-15 µl of 1% acetic acid was added to prenumbered microcentrifuge tubes for alkaline reactions between pH-levels 9 to 13.

2.1.3 HPLC Analysis

The samples were transferred from the original sample collection microtubes to corresponding HPLC sample vials. Analysis was carried out with Hewlett Packard Agilent 1100 or Perkin Elmer RP-HPLC analyzer, with Thermo Fisher Scientific™ Aquasil C18 columns (150 x 4mm, particle size 6 µm) and analysis was initialized in batches, one experiment at a time.

Mixtures of acetate buffer (0.030 M AcOH, 0.015 M NaOH, 0.1 M NH_4Cl) and HPLC grade acetonitrile were used as eluents. Due to differences in the analyzer features and a switch to a newer column, isocratic elution with 5% acetonitrile or gradient elution with variations in acetonitrile concentration from 0-30% were used. UV detection was conducted at wavelengths of 260, 270 and 280 nm, of which the wavelength of 270 nm was determined to be most suitable for the studied compounds.

2.2 Data analysis

The experimental data were further analyzed to determine parameters for the full kinetic analysis of the studied RNA model compounds, namely HPNP (**4a**), HPCP (**4b**) and HPHP (**4c**). The data analysis was divided into two parts: data processing with Origin statistical program and calculations. The information obtained from the statistical data processing was then applied to determine reaction kinetics parameters based on the integrated rate law for first-order chemical reactions.

2.2.1 Reaction Rate Constant determination

The reaction results recorded on individual test sheets from the phase one experiments for each RNA model compound at high- and low-end pH-levels at 25, 50, 75 and 90°C temperatures were plotted to Origin statistical program for further analysis. The rate constant (k) was calculated by applying an integrated first-order rate equation.

The additive inverse of the slope value equals the first order rate constant (k), as the graph is plotted with the natural logarithm of A ($\ln A$) against time is seconds (t). The variable A refers to any quantity proportional to the concentration, such as the start material peak area or mole fraction (63).

A linear fitting analysis was performed to form two separate graphs with Origin statistical program. One graph was based on the start material area (Graph. 1.), while the second was based on the molar fraction (Graph. 2.) in relation to reaction time in seconds. The data from the phase one experiments formed descending linear graphs.

In this study, the Start Material Area peak Graphs presented more precise interpretation of the reaction progression, as the formation of the product did not correlate directly with the depletion of start material. Consequently, the molar fraction graphs were created for comparative analysis, to assist at identifying potential experimental process errors, such as evaporation, reveal potential side reactions and incomplete start material conversion.

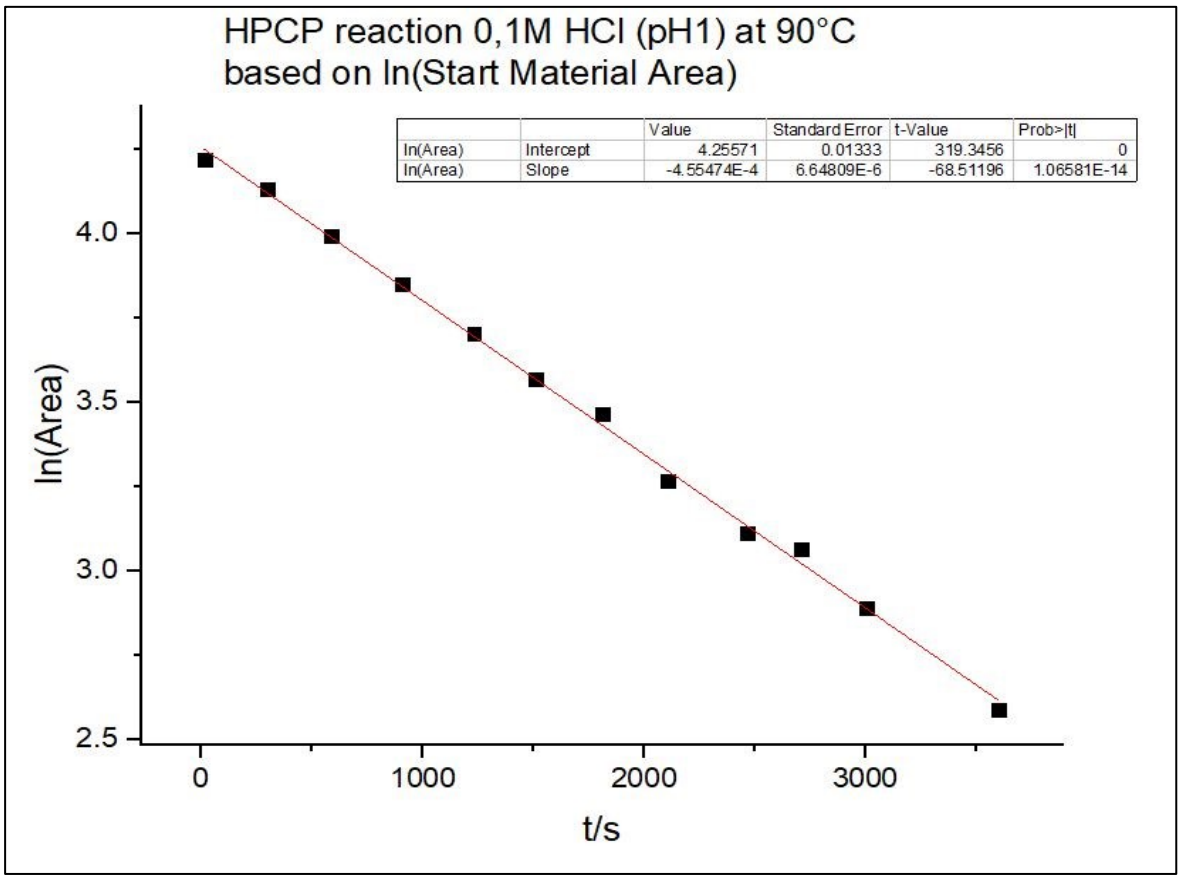

Graph. 1. Example of reaction data entering of HPCP(**4a**) reaction pH1 at 90 °C in which ln(Area) is plotted against time is seconds (t/s).

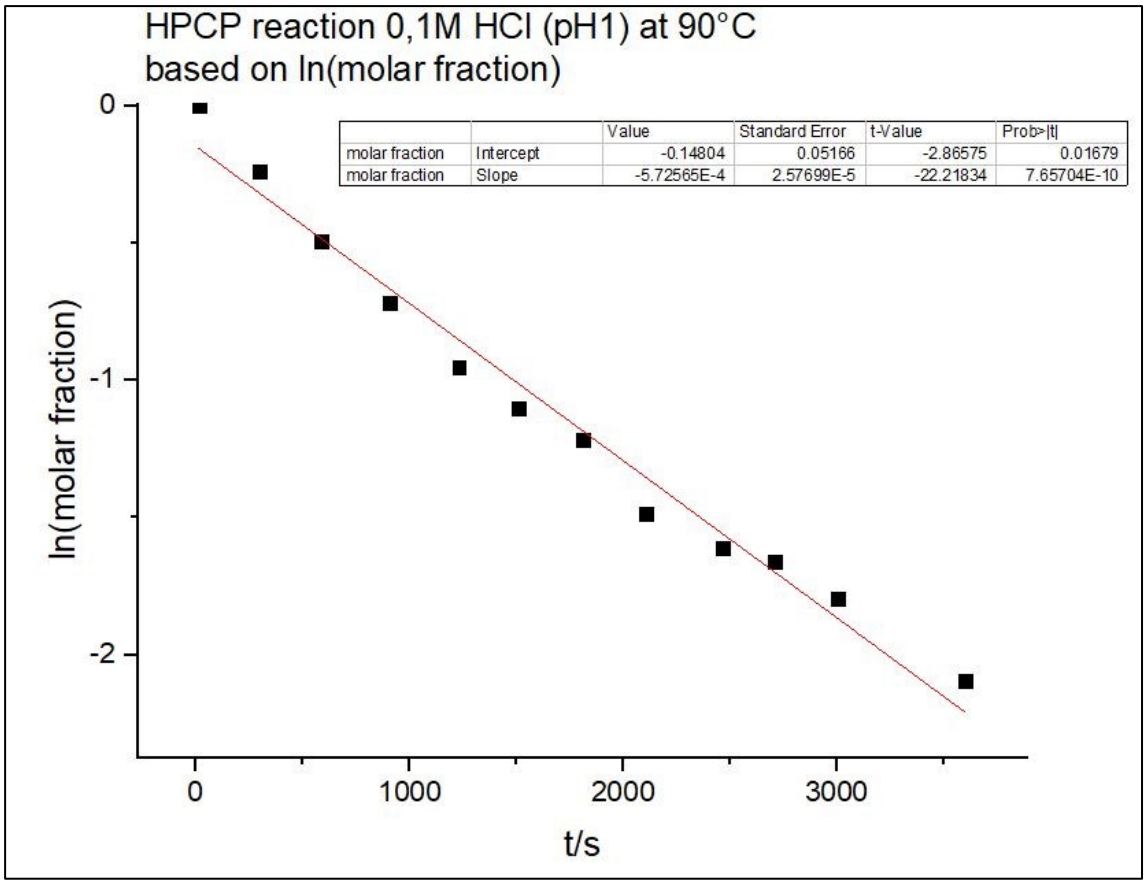

Graph. 2. Example of reaction data entering of HPCP(**4a**) reaction pH9 at 90 °C in which ln(molar fraction) is plotted against time is seconds (t/s).

2.3.2 Calculating the reaction activation parameters and β_{LG}-values

The reaction activation parameters were determined experimentally by plotting the natural logarithm of rate constant (ln*(k)*) against the inverse temperature in Kelvins (*1/T*) to determine the slope and y-intercept values. The Modified Eyring Equation was then applied to further determine the reaction activation parameters. In this equation, the slope equals the negative energy of activation divided by the gas constant (*-Ea/R*), while the y-intercept value represents the collision factor (ln*A*) as described in the literature (63). The Modified Eyring Equation was used to calculate the standard enthalpy ($\Delta H^{\neq}$) and entropy ($\Delta S^{\neq}$) of activation:

$$y - intercept = \frac{\Delta S^{\neq}}{R} \rightarrow \Delta S^{\neq} = y - intercept * R \text{ (63)}$$

$$slope = \frac{-\Delta H^{\neq}}{R} \rightarrow \Delta H^{\neq} = -slope * R \text{ (63)}$$

The intercept and slope values obtained from the Eyring equation graphs for each RNA model compound (Graph. 3) were utilized for reaction activation parameter calculations to determine

the activation energy, enthalpy, and entropy (see Appendix 2-4 Reaction activation parameter calculations).

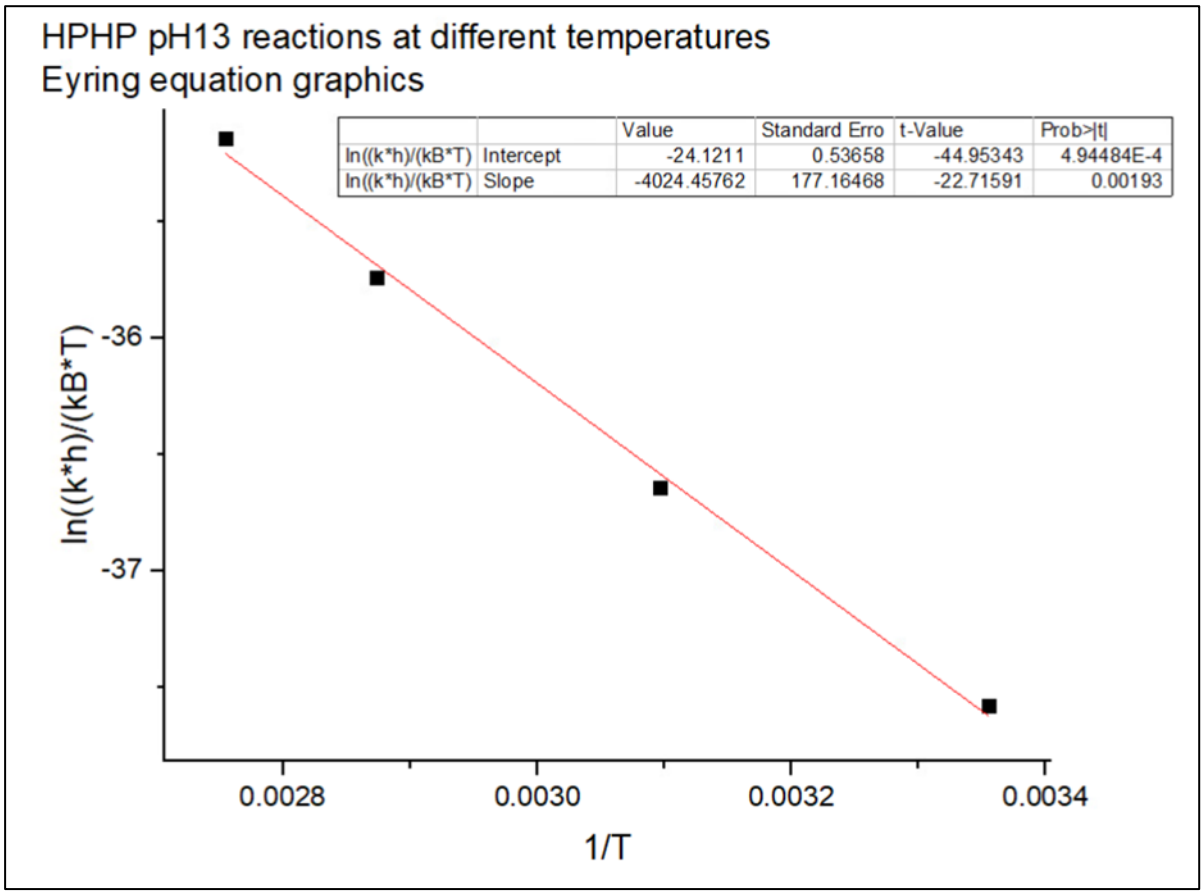

Graph. 3 Example of reaction rates temperature dependency of RNA model compound HPHP

The logarithmic rate constant *log(k)* from experiments performed at 90 °C for pH-levels 1, 5 and 9 for each model compound were plotted against the corresponding p*K*a-values of the leaving group (Table 3.). The linear Beta leaving group (β_{LG}) graphs (Graph. 4) represent that the numerical intercept value corresponds to the numerical β_{LG}-value at the known pH-level.

Table 3. Leaving group p*K*a-values at 25°C according to reference (39)

Model Compound	**Leaving Group**	**p*K*a (25°C)**
HPHP	Phenol	9.95
HPCP	2-Chlorophenol	8.48
HPNP(4a)	Para-nitrophenol	7.14

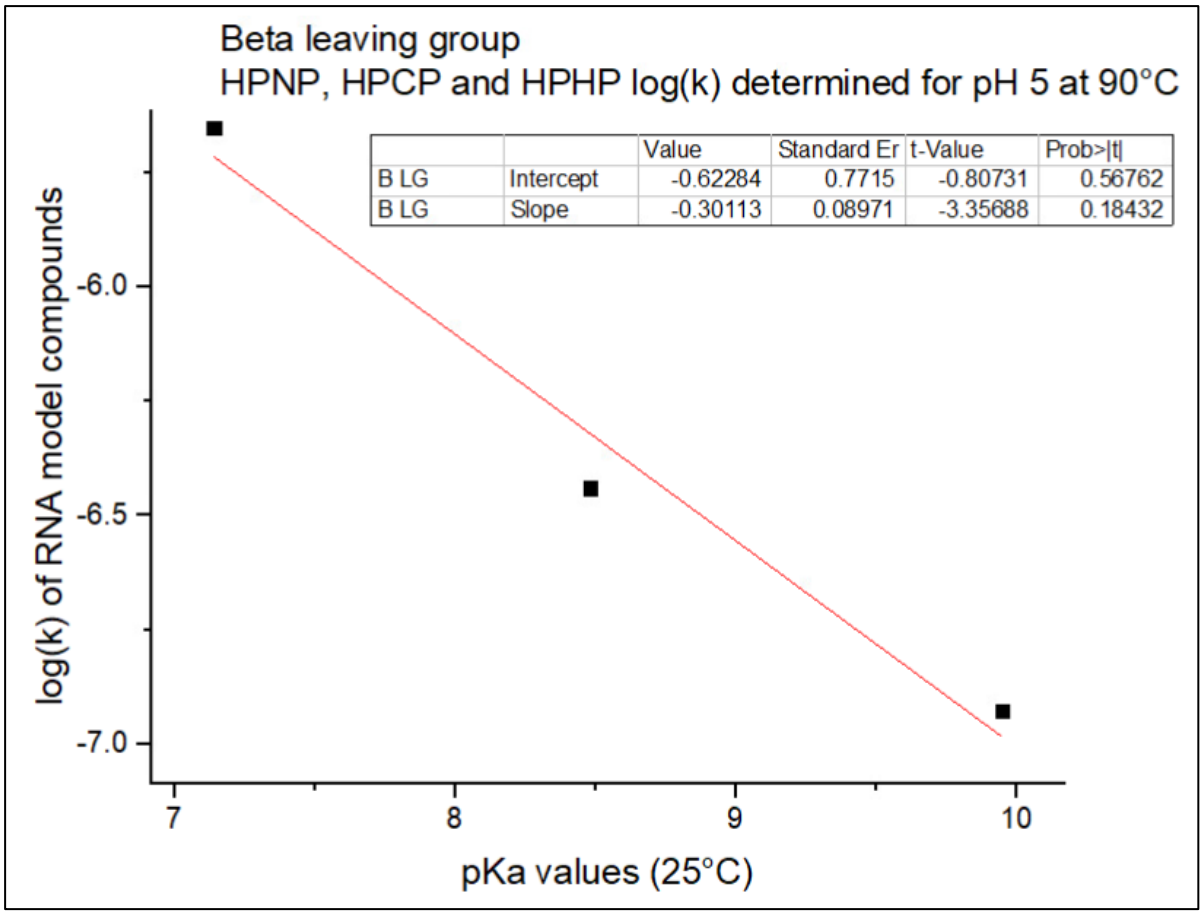

Graph. 4 Example of Beta leaving group graph

3 Results and Discussion

3.1 The effect of pH variation on 2-hydroxypropyl phosphates

The phosphodiester cleavage reaction of the studied model compounds was observed over a wide range pH-scale at 90°C. Each compound resulted in a similar transesterification outcome at the end point of the reaction. The transesterification led to the release of a phenol or a substituted phenol product, depending on features of the studied model compounds. No isomerism was observed for any of the model compounds.

The experimentally determined reaction rates for the studied compounds can be observed in the pH-rate profiles presented in Graph. 5. The upward-opening curve's shape and size are very similar for all three compounds. The transesterification reaction demonstrated accelerated reaction rates under both acidic and basic reaction environments, with similar reactivity minimum around pH 5.

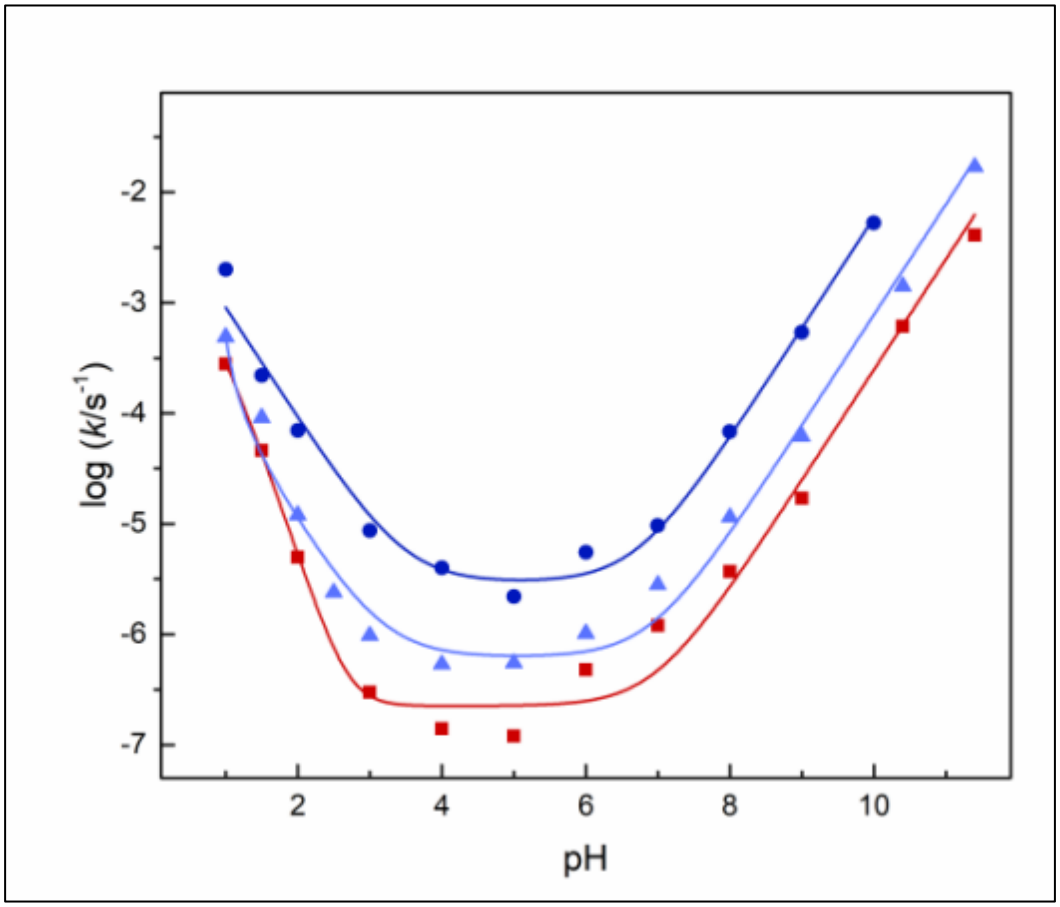

Graph. 5 2-hydroxypropyl phosphates pH-rate profiles at 90°C. Notation: HPNP (navy circles), HPCP (blue triangles) and HPHP (red Squares) (41)

All three model compounds presented a clear first-order hydroxide ion dependency in reaction environments above pH 7, as indicated by the linear increase in reaction rate with hydroxide ion concentration. The reaction rate slope plotted against the hydroxide ion concentration was found to be +1 further indicating a first-order reaction. Additionally, the constancy of the reactant half-life throughout the reaction, the exponential increase in the rate constant with temperature according to the Arrhenius equation, and the linearity of the plotted integrated rate law equation all support the conclusion of a first-order reaction.

The second-order dependency on acid concentration is observed more prominently for HPHP (**4c**) and HPCP (**4b**), as the relationship between reaction rate and concentration is steeper compared to HPNP (**4a**). This suggests that the mechanism in acid-catalyzed reactions appears to vary among the studied compounds. The impact of proton (H^+) concentration in the acidic reaction environment differs among the compounds, indicating that the increasing proton concentration affects the leaving groups distinctively.

HPCP (**4b)** exhibits similar pH-rate profile shape and reactivity as 3'5'-UpU (**1**) (46). In comparison, more structurally complex compound uridine 3'-(2-chlorophenyl) phosphate (UPCP, **3b**) (45) has shown significantly higher reactivity in previous studies. Evaluation of the leaving group and intramolecular nucleophile characteristics reveals that UPCP (**3b**) obtains both good leaving group and nucleophile properties, hence better reactivity.

Both 3'5'-UpU and 2-hydroxypropyl phosphates display an inverse relationship between their nucleophile and leaving group characteristics. 3'5'-UpU (**1**) obtains good nucleophilic properties but poor leaving group characteristics. In contrast, 2-hydroxypropyl phosphates (4) have better leaving group characteristics, indicating that they are more easily displaced in a reaction but resulting in poorer nucleophilicity. Despite the differences between the inversed relationship of 3'5'-UpU (**1**) and 2-hydroxypropyl phosphates (**4**) nucleophile and leaving group, the combined effects lead to surprisingly similar pH-rate profiles in comparison.

Reaction rate constants (Table 4.) decrease in the following order in all pH levels HPNP (**4a**) > HPCP (**4b**) > HPHP (**4c**), indicating that HPNP (**4a**) possesses the highest reactivity and dependency on pH changes. The simple, slim secondary alcohol chain of the compounds (**4a-c**) promotes structural mobility as it can easily flutter compared to nucleosides with 2'OH attached to a bulkier and rigid ring structure. However, the better the leaving group of the 2-hydroxypropyl phosphate, the more likely the nucleophilic attack initiates the reaction cascade,

hence hindering the fluttering. Furthermore, experimentally determined reaction rates can be considered quite reliable, as the buffered reaction medium and reaction environment monitoring were carried out throughout each reaction.

Table 4. Experimentally determined reaction rate constants (s^{-1}) for HPHP, HPCP and HPNP at 90 °C

pH	***k*(HPHP)s^{-1}**	***k*(HPCP)s^{-1}**	***k*(HPNP)s^{-1}**
1	2.8(±0.1) x10^{-4}	4.6(±0.07) x10^{-4}	2.0(±0.01) x10^{-3}
2	1.7(±1.5) x10^{-6}	1.2(±0.1) x10^{-5}	7.0(±0.08) x10^{-5}
3	3.0(±0.3) x10^{-7}	2.3(±0.2) x10^{-7}	8.7(±0.04) x10^{-6}
4	1.4(±0.2) x10^{-7}	2.2(±0.1) x10^{-7}	4.0(±0.1) x10^{-6}
5	1.2(±0.2) x10^{-7}	3.6(±0.2) x10^{-7}	2.2(±0.2) x10^{-6}
6	4.8(±0.8) x10^{-7}	6.6(±0.7) x10^{-7}	5.5(±0.3) x10^{-6}
7	1.2(±0.04) x10^{-6}	2.8(±0.2) x10^{-6}	9.6(±0.3) x10^{-6}
8	3.7(±0.03) x10^{-6}	5.4(±0.5) x10^{-6}	6.8(±0.2) x10^{-5}
9	1.7(±0.07) x10^{-5}	6.2(±0.3) x10^{-5}	5.4(±0.07) x10^{-4}
10	9.6(±0.4) x10^{-5}	5.5(±0.3) x10^{-5}	5.2(±0.06) x10^{-3}
11	4.0(±0.2) x10^{-4}	4.9(±0.1) x10^{-4}	N/A
12	6.1(±0.3) x10^{-4}	1.4(±0.2) x10^{-3}	N/A
13	4.1(±0.2) x10^{-3}	1.7(±0.05) x10^{-2}	N/A

The direct comparison of the results discovered in this study with previous studies is limited due to the lack of previous studies which would be directly proportional to the context of full kinetic analysis of 2-hydroxypropyl phosphates. However, some previous studies conducted with various phosphodiesters with diverse nucleophile and leaving group features were compared to the findings discovered in this study. Previous studies of 3'5'-UpU (**1**) (46) and UPCP (**3b**) (45) exhibited varied reactivity based on their structural features and functional groups.

The reactivity of 3'5'-UpU (**1**) (46) and HPCP (**4b**) follows a similar pH-rate profile shape. The combined effects lead to same results despite the differences between their nucleophile and leaving group features and overall reactivity. UPCP (**3b**) (45) reacts much more rapidly under

neutral and alkaline conditions, being 10^4 times faster than both HPCP (**4b**) and 3'5'-UpU (**1**) (46) in similar reaction environments. In addition to the reactivity differences, the second order dependency on hydronium ion concentration for UPCP (**3b**) (45) seems to be non-existent, indicating that the mechanism of reactivity is distinguishably different from HPCP (**4b**) and 3'5'-UpU (**1**) (46). With compounds allowing a more congruent comparison, such as methyl phosphate dianion (MMP) (64), the phosphodiester bond cleavage was estimated to be extremely slow with an estimated reaction rate of 2.0 $x10^{-20}$ s^{-1} (1 M KOH, 25 °C) (64).

As stated before, mechanism of reactions is highly dependent on the leaving group characteristics. The predicted proceeding of the reaction can be evaluated regarding the suitability of the leaving group. Substrates with poor leaving groups tend to react at late transition state with stepwise mechanism. More acidic and labile leaving groups tend to lower both early and later transition states (37).

The leaving groups' p*K*a values align with the observed reactivity of the compounds, in which the fast-reacting HPNP (**4a**) p-nitrophenol features a lower p*K*a value of 7.14, while intermediately reacting HPCP (**4b**) 2-Chlorophenol p*K*a value is 8.45 and the slowest reacting compounds HPHP (**4c**) phenol leaving group has the highest p*K*a value of 9.95.

The beta leaving group values provide an additional insight to the reactivity trends. The results suggest that the β_{LG} values determined in different reaction media at 90 °C increase modestly proceeding the reaction from acidic to alkaline conditions. The calculated beta leaving group values vary slightly between different pH levels: –0.30(±0.1) at pH 1, –0.45(±0.1) at pH 5, and –0.53(±0.1) at pH 9. These values obtained under alkaline conditions are consistent with the finding by Brown and Usher (59), who reported similar β_{LG} values of –0.56 (50 mM NaOH, 80 °C) for hydroxyalkyl phosphate esters (59).

A study conducted by Davis *et al*. (44) with nucleotide based aryl phosphates revealed β_{LG} values of –0.54 (Specific base catalyzed, 50 °C), and –0.59 (General base catalyzed, 50 °C) (44). The β_{LG} values of 2-hydroxypropyl phosphates determined for the base catalyzed reactions are fairly similar with β_{LG} values of –0.45(±0.1) and –0.53(±0.1), respectively.

Mikkola *et al*. (50) determined that aryl phosphates in acid-catalyzed reaction environments showed β_{LG} values of –0.27 (0.1 M HCl, 90 °C) and –0.2 (0.1 M HCOOH buffer, pH 3.5, 90 °C). These β_{LG} values indicate that the stability of the leaving group varies from moderate to weak (50). However, the comparison of β_{LG} values for aryl phosphates (50) present similarities

with this study, as the values are not significantly different. In the context of esters, alkyl esters feature aliphatic leaving groups and aryl esters aromatic leaving groups. This

A study by Kosonen *et al*. (49) of nucleoside 3'-alkylphosphates showed even higher variation between acid- and base-catalyzed reactions. β_{LG} values of –1.28 (HO^- catalyzed cleavage, 90 °C) and –0.12 (H_3O^+ catalyzed cleavage, 90 °C) (49) were determined, indicating a wide variability in β_{LG} values for dinucleoside monophosphates compared to other compounds, such as esters. However, in the context of esters, the differences between alkyl esters featuring aliphatic leaving groups with straight chain structures versus ring-shaped aryl esters containing aromatic leaving groups should be noted, as their chemical properties and reactivity are different.

3.2 The activation parameters of reaction dynamics

The reaction rate constants of 2-hydroxypropyl phosphates were determined at different temperatures and provided the basis for activation parameter calculations presented in table 5. The comprehensive review of the reactivity of 2-hydroxypropyl phosphates reaction dynamics is based on the transition state theory, which utilizes the relationship between reaction rate and the transition state of the reaction (65). The transition state theory includes individual elementary steps, such as statistic thermodynamics, rather than sole temperature dependence of the reaction rate phenomena, contrary to the Arrhenius theory (66).

The hypothesis of the transition state theory includes an equilibrium between the starting material and the transition state, which decomposes into products with a certain probability. These probabilities can be described as activation parameters, which are determined by measuring the rate of chemical reactions at different temperatures. The experimental observations can be translated into numerical activation parameter values by exploiting the Eyring equation (63; 66).

Enthalpy of activation ($\Delta H^{\neq}$) describes the energy difference between the transition state and starting material, hence the energy barrier required for the product transformation to occur (66). Enthalpy describes the enthalpy difference between highest energy point of the reaction at the transition state of the reaction and the reactants. A positive $\Delta H^{\neq}$ -value indicates that the system absorbs heat from the environment as the reaction moves from the initial state to the transition state. A negative $\Delta H^{\neq}$ -value indicates heat release to the reaction environment as the reaction

proceeds from the transition state to product, suggesting lower energy barrier and faster reaction rate (65; 66).

Entropy of activation ($\Delta S^{\neq}$) describes the level of disorder between the transition state and the initial reactants composition. Molecular movement and disorder typically increase as the old bonds break and new bonds start to form. However, in some cases, the molecular movement can decrease or remain constant depending on the specific reaction mechanism (66). A positive $\Delta S^{\neq}$ -value indicates that the reaction is dissociative, in which the transition state is more disordered. A negative $\Delta S^{\neq}$ -value indicates an associative reaction, in which the reacted components are more organized in structure as the system reaches the transition state (63; 65).

The level of entropy is strongly solvent dependent, as the properties of some solvents can modulate the reaction kinetics. The properties of the solvents, including its hydrogen bonding abilities, polarity and viscosity may affect the overall molecular movement of the reactants. Additionally, these properties can change with variations in reaction temperature. These temperature initiated changes in solvents properties can alter the transition state structure and entropy of activation, ultimately affecting the overall reaction kinetics. (63; 65).

Table 5. Experimental Reaction Activation parameters for HPHP, HPCP and HPNP

Compound	**Reaction**	***Ea*** **(kJ mol^{-1})**	**ln*A***	**$\Delta H^{\neq}$** **(kJ mol^{-1})**	**$\Delta S^{\neq}$** **(J K^{-1} mol^{-1})**
HPHP	pH 1	81.54	18.71	78.81	–98.45
	pH 13	36.18	6.48	33.46	–200.5
HPCP	pH 1	95.69	24.01	92.96	–54.37
	pH 13	51.6	13.08	48.88	–145.3
HPNP	pH 1	80.17	19.99	14.31	–268.1
	pH 10	94.49	27.28	93.76	–27.18

Upon closer examination of the reaction activation parameters, the calculated findings align with the experimentally observed reactivity features of the studied model compounds. Both activation energy (*Ea*) and enthalpy ($\Delta H^{\neq}$) rise with the leaving group favorability, in which higher electronegativity aligns with better leaving group character. However, the calculated

values at pH 1 may not be directly comparable to values determined in alkaline conditions due to different reaction rate dependencies on acid concentration.

The observed variations in reaction rate dependency in acidic conditions are attributed to slight differences in reaction mechanisms between the studied model compounds. Therefore, the reaction activation parameters determined for pH 1 should be noted as suggestive evidence. However, a clear trend can be observed in the reaction activation energies (*Ea*), with acid-catalyzed reactions exhibiting higher values than base-catalyzed reactions.

In general, all 2-hydroxypropyl phosphate systems have positive enthalpy ($\Delta H^{\neq}$) values in acidic and alkaline reaction medium. This indicates that the active reaction system absorbs heat from the reaction environment, in which the severity of the energy barrier varies in between the studied compounds. HPNP (**4a**) with p-nitrophenol as leaving group presents somewhat different enthalpy findings compared to HPCP (**4b**) and HPHP (**4c**). Results under the alkaline conditions reveal that HPHP (**4c**) and HPCP (**4b**) show decreased enthalpy in pH 13 compared to HPNP (**4a**) in pH 10.

All activation reaction entropy ($\Delta S^{\neq}$) values are negative, which confirms the initial assumption of an associative reaction outcome. In basic conditions, a clear trend is observed as the activation entropy becomes less negative, which aligns with the leaving group character becoming more favorable. This indicates a change in the nature of the reaction from associative towards more concerted. P-nitrophenol (HPNP, **4a**) as leaving group has superior reaction energetics under alkaline conditions compared to phenol and 2-chlorophenol, making the reaction more energetically favorable and less endothermic.

4 Conclusion

Based on the experimental results, the studied model compounds demonstrate similar reactivity patterns, as shown by the shape and scale of the pH-rate-profiles. Both acidic and basic reaction environment catalyze the transesterification reaction for the studied compounds. Notably, alkaline and neutral reaction conditions highlight the effect of leaving group differences, as compounds with better leaving group exhibit faster reactivity. The reactivity correlates with nucleophilicity. Similar reactivity features were observed in acidic reaction conditions, with proportional differences in comparison. These findings align with previous studies conducted with similar small molecular models. The reaction activation parameters further support these findings.

The studied compounds present suboptimal comparison to the transesterification reaction of naturally occurring RNA due to simplified nucleophiles and leaving groups, which have opposing features in comparison. However, this newfound information can be utilized in the artificial phosphodiester model compound development, since the structural features of the studied compounds provided new insight into which characteristics are more favorable. Additionally, this study presents the first full kinetic analysis ever reported for the studied compounds of 2-hydroxypropyl phosphates.

The results of this thesis provide valuable new insights into the transesterification reaction of 2-hydroxypropyl phosphates and contribute to the ongoing investigations of the phosphodiester bond reactions from a general perspective. Future research directions of 2-hyrdoxypropyl phosphates could explore their usability for metal-complex catalyzed applications.

References

1. Zhu, Y.; Zhu, L.; Wang, X.; Jin, H., *Cell Death Dis.,* **2022**, *13*, 1–15.

2. Yu, A.-M.; Choi, Y. H.; Tu, M.-J., *Pharmacol. Rev.,* **2020**, *72*, 862–898.

3. Weeks, K. M., *Curr. Opin. Struct. Biol.,* **2010**, *20*, 295–304.

4. Sparmann, A.; Vogel, J., RNA-based medicine: from molecular mechanisms to therapy. *EMBO J.* [online] **2023**, *42*, e114760. Avalaible at: https://doi.org/10.15252/embj.2023114760 (Accessed: 14.03.2024).

5. Chatterjee, S.; Bhattacharya, M.; Lee, S.-S.; Chakraborty, C., *Curr.Res. Biotechnol.,* **2023**, *12*, 757–758.

6. Connelly, C. M.; Moon, M. H.; Schneekloth, J. S., *Cell Chem. Biol.,* **2016**, *23*, 1077–1090.

7. Lönnberg, H., *Org. Biomol. Chem.,* **2011**, *9*, 1687–1703.

8. Mikkola, S.; Lönnberg, T.; Lönnberg, H., *Beilstein J. Org. Chem.,* **2018**, *14*, 803–837.

9. Genome: *Nucleic-Acids*. Bates, S., https://www.genome.gov/genetics-glossary/Nucleic-Acids (accessed 2023-04-01).

10. Blanco, A.; Blanco, G. *Medical Biochemistry*, 1st ed.; Academic Press; Cambridge, Massachusetts, 2017, pp. 121–140.

11. Minchin, S.; Lodge, J., *Essays Biochem.,* **2019**, *63*, 433–456.

12. Neidle, S.; Sanderson, M. *Principles of Nucleic Acid Structure*, 2nd ed.; Academic Press; London, England, 2022, pp. 29–51.

13. Morris, J.; Hartl, D.; Knoll, A.; Lue, R.; Michael, M.; Berry, A.; Biewener, A.; Farrell, B.; Holbrook, M. *Biology How Life Works*, 3rd ed.; Macmillan International Higher Education: New York, 2019, pp. 51–68.

14. Halder, S.; Bhattacharyya, D., *Prog. Biophys. Mol. Biol.,* **2013**, *113*, 264–283.

15. Ramos, S. B. V.; Laederach, A., *Nature,* **2014**, *505*, 621–622.

16. Macke, T. J., *Nucleic Acids Res.,* **2001**, *29*, 4724–4735.

17. Šponer, J. E.; Špačková, N.; Leszczyński, J.; Šponer, J., *J. Phys. Chem.,* **2005**, *109*, 11399–11410.

18. Leontis, N. B.; Westhof, E., *RNA* **2001**, *7*, 499–512.

19. Ohi, M. D. *Methods* **2017**, *125*, 1046-2023.

20. Šponer, J.; Bussi, G.; Krepl, M.; Banáš, P.; Bottaro, S.; Cunha, R. A.; Gil-Ley, A.; Pinamonti, G.; Poblete, S.; Jurečka, P.; Walter, N. G.; Otyepka, M., *Chem. Rev.,* **2018**, *118*, 4177–4338.

21. Phaniendra, A.; Jestadi, D. B.; Periyasamy, L., *Indian J. Clin. Biochem.,* **2014**, *30*, 11–26.

22. Tanaka, M.; Chock, P. B., *Front. Mol. Biosci.,* **2021**, *8*, 1–13.

23. Hofer, T.; Badouard, C.; Bajak, E.; Ravanat, J.-L.; Mattsson, Å.; Cotgreave, I. A., *Biol. Chem.,* **2005**, *386*, 333–337.

24. Kong, Q.; Lin, C. G., *Cell. Mol. Life Sci.,* **2010**, *67*, 1817–1829.

25. Elliott, D.; Ladomery, M. *Molecular Biology of RNA*, 2nd ed.; Oxford University Press: New York, 2017; pp. 29–51.

26. Voet, D.; Voet, J. G. *Biochemistry*, 4th ed.; John Wiley And Sons: Hoboken, N.J., 2011; pp. 67–75.

27. Kuusela, S.; Lönnberg, H. *J. Chem. Soc., Perkin Trans. 2.,* **1994**, 10, 2109–2113.

28. Akiba, K.-Y. *Organo Main Group Chemistry*; Wiley & Sons: Hoboken, N.J., 2011, pp. 111–158.

29. Umuhire Juru, A.; Hargrove, A. E., *J. Biol. Chem.,* **2021**, *296*, 1–12.

30. DeWeerdt, S., *Nature,* **2019**, *574*, S2–S3.

31. Perreault, D. M.; Anslyn, E. V., *Angew. Chem. Int. Ed.,* **1997**, *36*, 432–450.

32. Lönnberg, H., *Chem. Rec.,* **2022**, *22*, 1–17.

33. Dissanayake, T.; Swails, J. M.; Harris, M. E.; Roitberg, A. E.; York, D. M., *Biochem.,* **2015**, *54*, 1307–1313.

34. Korhonen, H.; Williams, N. H.; Mikkola, S., *J. Phys. Org. Chem.,* **2012**, *26*, 182–186.

35. Schnieders, R.; Keyhani, S.; Schwalbe, H.; Fürtig, B., *Chem. Eur. J.,* **2019**, *26*, 102–113.

36. Jackson, R. W.; Smathers, C. M.; Robart, A. R., *Molecules,* **2023**, *28*, 2111–2111.

37. Huang, M.; York, D. M., *Phys. Chem. Chem. Phys.,* **2014**, *16*, 15846–15855.

38. Lössl, P.; Van De Waterbeemd, M.; Heck, A. J., *EMBO J.,* **2016**, *35*, 2634–2657.

39. Korhonen, H.; Koivusalo, T.; Toivola, S.; Mikkola, S., *Org. Biomol. Chem.,* **2013**, *11*, 8324–8324.

40. Leamy, K. A.; Assmann, S. M.; Mathews, D. H.; Bevilacqua, P. C., *Q. Rev. Biophys.,* **2016**, *49*, 1–26.

41. Koski, J. I.; Poijärvi, E.; Tulisalo, A.; Mikkola, S. *The Cleavage of RNA Model Compounds: The Interplay between the Nucleophile and the Leaving Group*; Unpublished Article: University of Turku, 2024.

42. Cassano, A. G.; Anderson, V. E.; Harris, M. E., *Biopolymers,* **2003**, *73*, 110–129.

43. Kosonen, M.; Yousefi-Salakdeh, E.; Strömberg, R.; Lönnberg, H., *J. Chem. Soc.,* **1998**, *7*, 1589–1596.

44. Davis, A. M.; Hall, A. D.; Williams, A., *J. Am. Chem. Soc.,* **1988**, *110*, 5105–5108.

45. Oivanen, M.; Kuusela, S.; Lönnberg, H., *Chem. Rev.,* **1998**, *98*, 961–990.

46. Järvinen, P.; Oivanen, M.; Lönnberg, H., *J. Org. Chem.,* **1991**, *56*, 5396–5401.

47. Xu, Y.; Harris, M. E.; York, D. M.; Wong, K.-Y., *J. Chem. Theory Comput.,* **2023**, *19*, 1322–1332.

48. Kosonen, M.; Seppänen, R.; Wichmann, O.; Lönnberg, H., *J. Chem. Soc., Perkin Trans. 2,* **1999**, *11*, 2433–2439.

49. Kosonen, M.; Youseti-Salakdeh, E.; Strömberg, R.; Lönnberg, H., *J. Chem. Soc.,* **1997**, *12*, 2661–2666.

50. Mikkola, S.; Stenman, E.; Nurmi, K.; Yousefi-Salakdeh, E.; Strömberg, R.; Lönnberg, H., *J. Chem. Soc., Perkin Trans. 2,* **1999**, *8*, 1619–1626.

51. Almer, H.; Strömberg, R., *J. Am. Chem. Soc.,* **1996**, *118*, 7921–7928.

52. Ora, M.; Hanski, A., *Helv. Chim. Acta.,* **2011**, *94*, 1563–1574.

53. Ye, J.-D.; Li, N.-S.; Dai, Q.; Piccirilli, J. A., *Angew. Chem. Int. Ed.,* **2007**, *46*, 3714–3717.

54. Bonfá, L.; Gatos, M.; Mancin, F.; Tecilla, P.; Tonellato, U., *Inorg. Chem.,* **2003**, *42*, 3943–3949.

55. Livieri, M.; Mancin, F.; Tonellato, U.; Chin, J., *Chem. Commun.,* **2004**, *24*, 2862–2862.

56. Korhonen, H.; Mikkola, S.; Williams, N. H., *Chem. Eur. J.,* **2012**, *18*, 659-670.

57. Korhonen, H. *The Significance of Hydrogen Bonding Interactions in the Cleavage of RNA.* Doctoral Thesis, University of Turku, 2011.

58. Tjioe, L.; Joshi, T.; Graham, B.; Spiccia, L., *Polyhedron.,* **2016**, *120*, 11–17.

59. Brown, D. M.; Usher, D. A., *J. Chem. Soc. (Resumed).,* **1965**, 6558–6564.

60. Rumble, J. R.; Bruno, T. J.; Doa, M. J. *CRC Handbook of Chemistry and Physics : A Ready-Reference Book of Chemical and Physical Data*, 95th ed.; Crc Press/Taylor & Francis Ltd: Boca Raton, 2014, pp. 972–981.

61. Virtanen, N.; Polari, L.; Välilä, M.; Mikkola, S., *J. Phys. Org. Chem.,* **2005**, *18*, 385–397.

62. Virtanen, N.; Nevalainen, V.; Lehtinen, T.; Mikkola, S., *J. Phys. Org. Chem.,* **2007**, *20*, 72–82.

63. Maskill, H. *The Physical Basis of Organic Chemistry*, 1st ed.; Oxford University Press USA: Oxford, 1985, pp. 244–245.

64. Duarte, F.; Åqvist, J.; Williams, N. H.; Lynn, C., *J. Am. Chem. Soc.,* **2014**, *137*, 1081–1093.

65. UC Davis Chemistry Libre Texts: *Physical & Theoretical Chemistry*. Johns, D.; Hutton, A. https://chem.libretexts.org/Bookshelves/Physical_and_Theoretical_Chemistry_Textbook_Maps (Accessed 11.09.2020).

66. UC Davis Chemistry Libre Texts: *9.7: Theories of Reaction Rates*. Dao, P.; Latif, B.; Zhao, L. https://chem.libretexts.org/Bookshelves/Physical_and_Theoretical_Chemistry_Textbook_Maps/Map%3A_Physical_Chemistry_for_the_Biosciences_(Chang)/09%3A_Chemical_Kinetics/9.07%3A_Theories_of_Reaction_Rates (Accessed 11.09.2020).

Appendices

Appendix 1 Pre-filled Test Sheet example

HPCP TEST 1

DATE: DD/MM/YY

HPCP reaction pH-level: 13
Reaction solution: 2,5 ml preheated 0,1 M NaOH
Water incubator temperature: 90°C

Micro vial tubes on ice bath with 15µl of HOAc
Pipette 150 µl of sample to corresponding micro vial.
HPLC Settings: PerkinElmer analyser
Method: Jasmin2

SAMPLE	TIME (min:sec)	TIME IN SEC	HPLC FILENAME /SAMPLE INFO	START MATERIAL TIME	START MATERIAL PEAK AREA	PRODUCT TIME	PRODUCT PEAK AREA	OTHER TIME/PEAK AREA
primary solution addition	00:00							
1	00:04	4	TEST1.1	3.000	100.000	7.000	----	n/a
2	00:10	10	TEST1.2	3.002	90.000	6.999	10.000	
3	00:15	15	TEST1.3	3.000	80.000	7.000	20.000	
4	00:30	30	TEST1.4	3.000	65.000	7.001	35.000	
5	00:40	40	TEST1.5	3.003	50.000	7.000	50.000	
6	00:50	50	TEST1.6	3.000	45.000	7.000	55.000	
7	01:00	60	TEST1.7	2.999	40.000	6.998	60.000	
8	01:15	75	TEST1.8	3.000	30.000	7.000	70.000	
9	01:30	90	TEST1.9	3.002	20.000	6.990	80.000	
10	02:00	120	TEST1.10	3.001	10.000	7.000	90.000	
11								
12								

Appendix 2 Reaction activation parameter calculations for HPHP

HPHP reaction series for 0.1 M NaOH (pH 13) derived from tests conducted in temperatures 25, 50, 75 and 90°C:

	A(X)	B(Y)	C(Y)	D(Y)	E(Y)	F(Y)	H(Y)
Long Name	t/C	k (pH13)	T/K	1/T	h	KB	ln((k*h)/(kB*T)
Units							
Comments		source area slopes		x-akseli	Planckin vakio	Boltzmanin vakio	y-akseli
F(x)=			273+col(A)	1/col(C)			ln((col(B)*col(E))/((col(F)*col(C))))
1	25	2.96E-4	298	0.00336	6.6262E-34	1.38E-23	-37.58173
2	50	8.23E-4	323	0.0031	6.6262E-34	1.38E-23	-36.63969
3	75	0.00218	348	0.00287	6.6262E-34	1.38E-23	-35.74012
4	90	0.00415	363	0.00275	6.6262E-34	1.38E-23	-35.13854

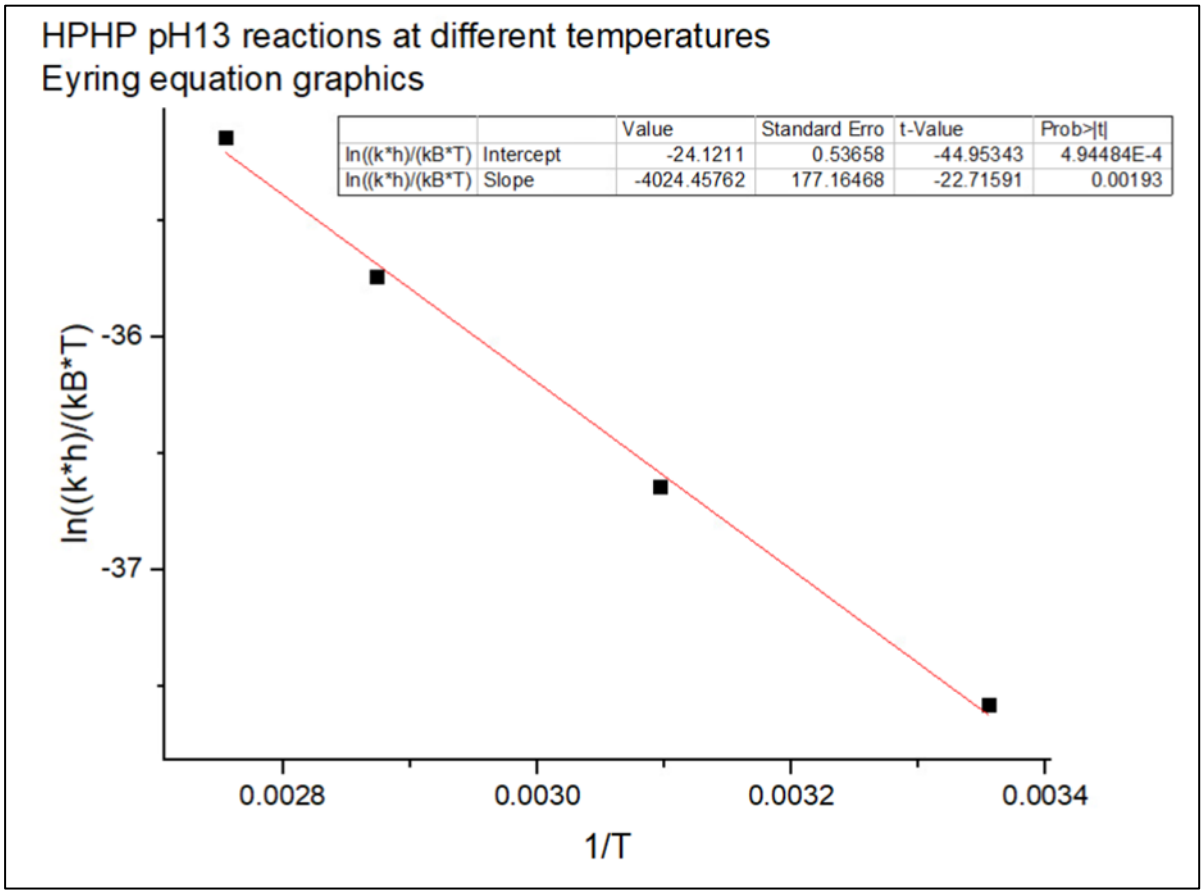

$$y - intercept = \frac{\Delta S^{\neq}}{R} \rightarrow \Delta S^{\neq} = y - intercept * R$$

$$\Delta S^{\neq} = y - intercept * R = -24{,}1211 * 8{,}314\ J\ mol^{-1}K^{-1} \approx -200{,}5\ J\ mol^{-1}K^{-1}$$

$$slope = \frac{-\Delta H^{\neq}}{R} \rightarrow \Delta H^{\neq} = -slope * R$$

$$\Delta H^{\neq} = -slope * R = -(-4024{,}45762) * 8{,}314\ J\ mol^{-1}K^{-1} \approx 33{,}46\ kJ/mol$$

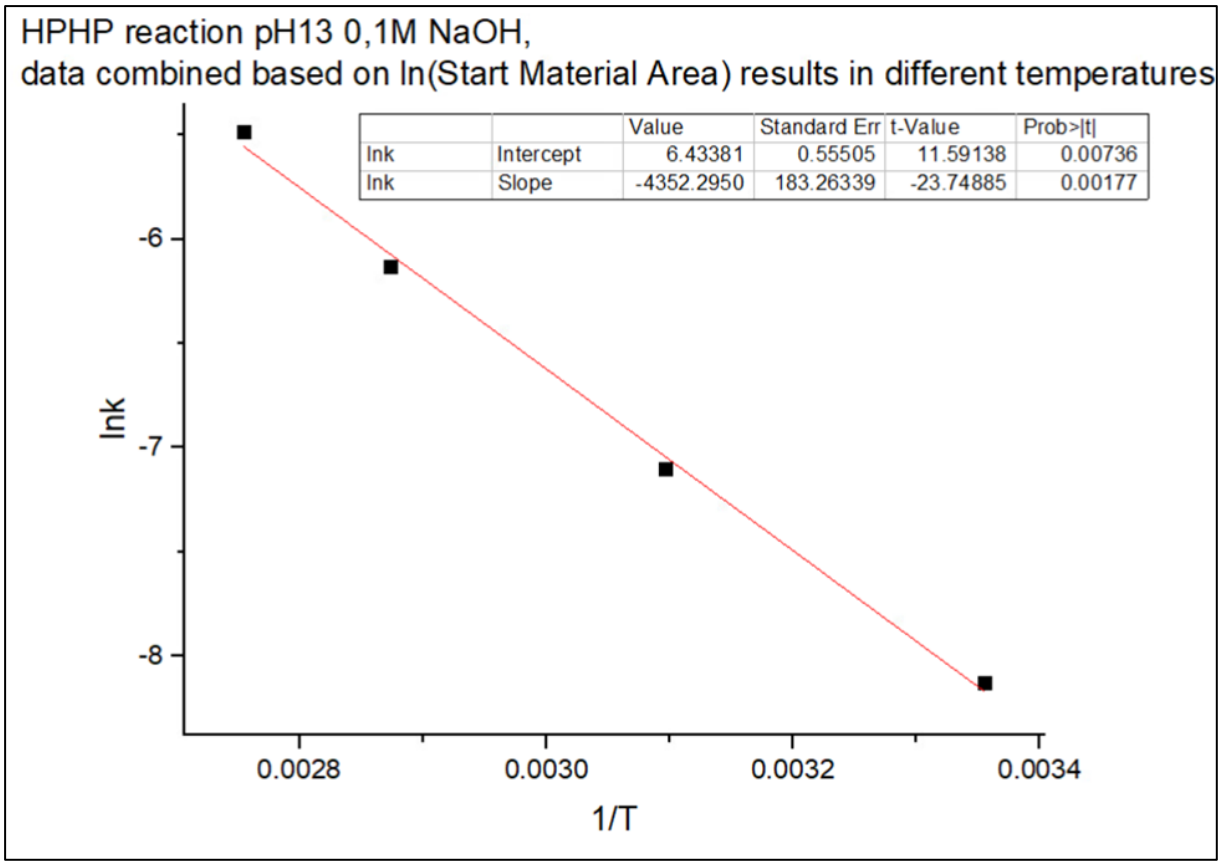

		Value	Standard Err	t-Value	Prob>|t|
lnk	Intercept	6.43381	0.55505	11.59138	0.00736
lnk	Slope	-4352.2950	183.26339	-23.74885	0.00177

$y - intercept = \ln A$

$A = e^{\ln A} = 2{,}718^{6{,}43381} = 616{,}259101 \approx 6{,}162 * 10^2$

$slope = -\frac{Ea}{R} \rightarrow Ea = -slope * R$

$Ea = -slope * R = -(-4352{,}2950) * 8{,}314\ J\ mol^{-1}K^{-1} \approx 36{,}18\ kJ/mol$

HPHP reaction series for 0.1 M HCl (pH 1) derived from tests conducted in temperatures 25, 50, 75 and 90°C:

	A(X)	B(Y)	C(Y)	D(Y)	E(Y)	F(Y)	G(Y)
Long Name	t/C	k (pH1)	T/K	1/T	h	KB	ln((k*h)/(kB*T)
Units							
Comments		source area slopes		x-akseli	Planckin vakio	Boltzmanin vakio	y-akseli
F(x)=			273+col(A)	1/col(C)			ln((col(B)*col(E))/((col(F)*col(C))))
1	25	7.73645E-7	298	0.00336	6.6262E-34	1.38E-23	-43.52873
2	50	7.12276E-6	323	0.0031	6.6262E-34	1.38E-23	-41.38936
3	75	7.315E-5	348	0.00287	6.6262E-34	1.38E-23	-39.13469
4	90	2.82015E-4	363	0.00275	6.6262E-34	1.38E-23	-37.82744

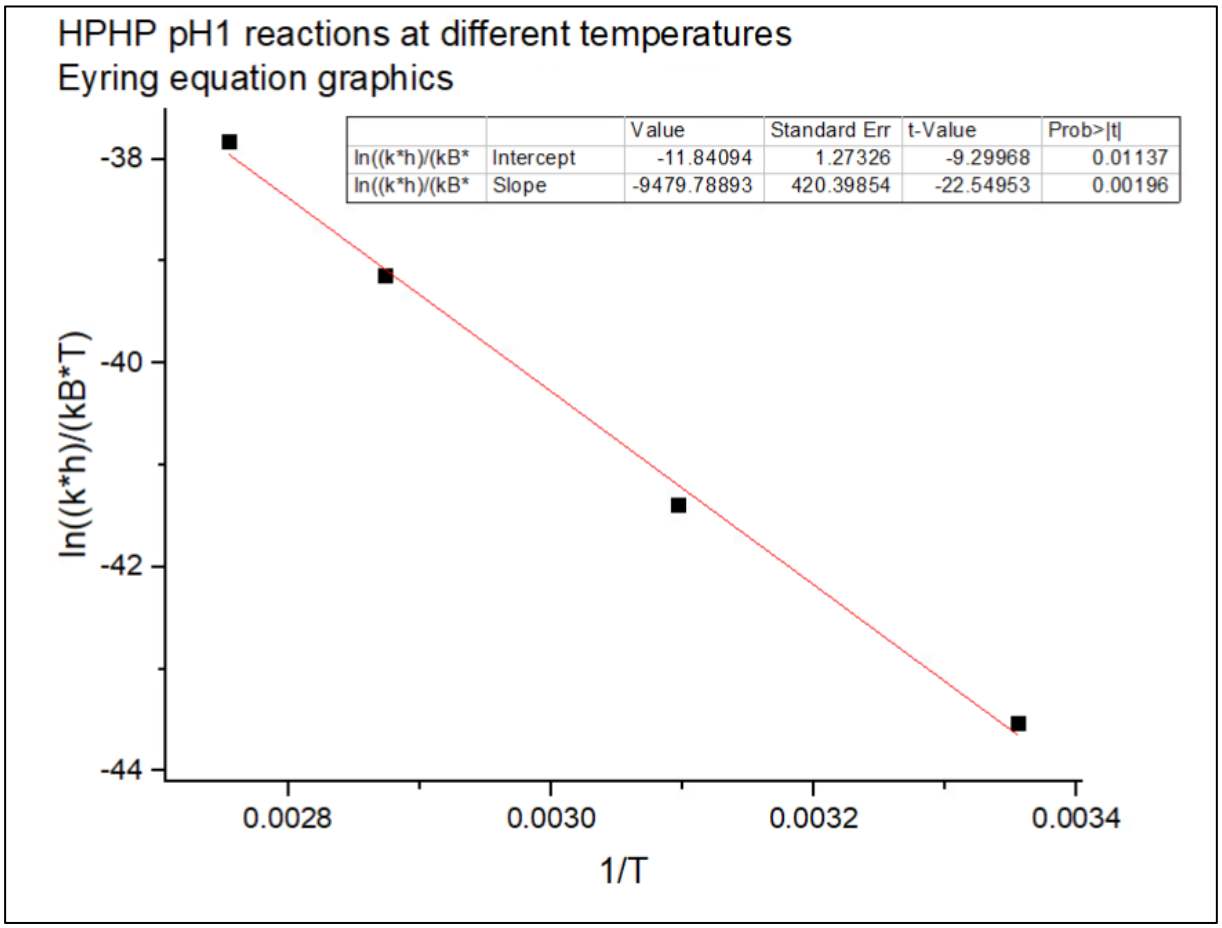

$$y - intercept = \frac{\Delta S^{\neq}}{R} \rightarrow \Delta S^{\neq} = y - intercept * R$$

$$\Delta S^{\neq} = y - intercept * R = -11{,}84094 * 8{,}314\, J\, mol^{-1}K^{-1} \approx -98{,}45\, J\, mol^{-1}K^{-1}$$

$$slope = \frac{-\Delta H^{\neq}}{R} \rightarrow \Delta H^{\neq} = -slope * R$$

$$\Delta H^{\neq} = -slope * R = -(-9479{,}78893) * 8{,}314\, J\, mol^{-1}K^{-1} \approx 78{,}81\, kJ/mol$$

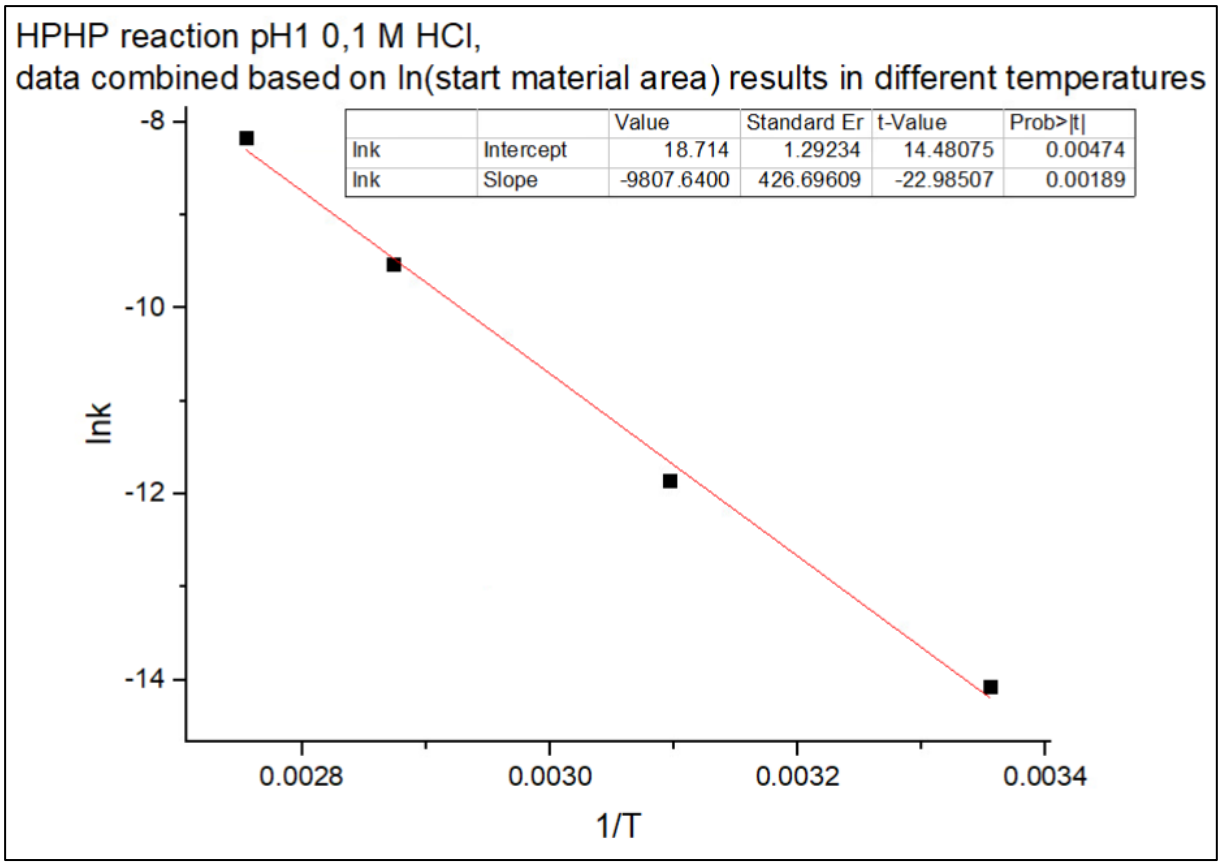

$y - intercept = \ln A$

$A = e^{\ln A} = 2{,}718^{18{,}714} = 133827157 \approx 1{,}338 * 10^{8}$

$slope = -\frac{Ea}{R} \rightarrow Ea = -slope * R$

$Ea = -slope * R = -(-9807{,}6400) * 8{,}314\ J\ mol^{-1}K^{-1} \approx 81{,}54\ kJ/mol$

Appendix 3 Reaction activation parameter calculations for HPCP

HPCP reaction series for 0.1 M NaOH (pH 13) derived from tests conducted in temperatures 25, 50, 75 and 90°C:

	A(X)	B(Y)	C(Y)	D(Y)	E(Y)	F(Y)	H(Y)
Long Name	t/C	k (pH13)	T/K	1/T	h	KB	ln((k*h)/(kB*T)
Units							
Comments		source area slopes		x-akseli	Planckin vakio	Boltzmanin vakio	y-akseli
F(x)=			273+col(A)	1/col(C)			ln((col(B)*col(E))/((col(F)*col(C))))
1	25	4.24412E-4	298	0.00336	6.6262E-34	1.38E-23	-37.22139
2	50	0.00221	323	0.0031	6.6262E-34	1.38E-23	-35.6519
3	75	0.00907	348	0.00287	6.6262E-34	1.38E-23	-34.31447
4	90	0.0172	363	0.00275	6.6262E-34	1.38E-23	-33.71674

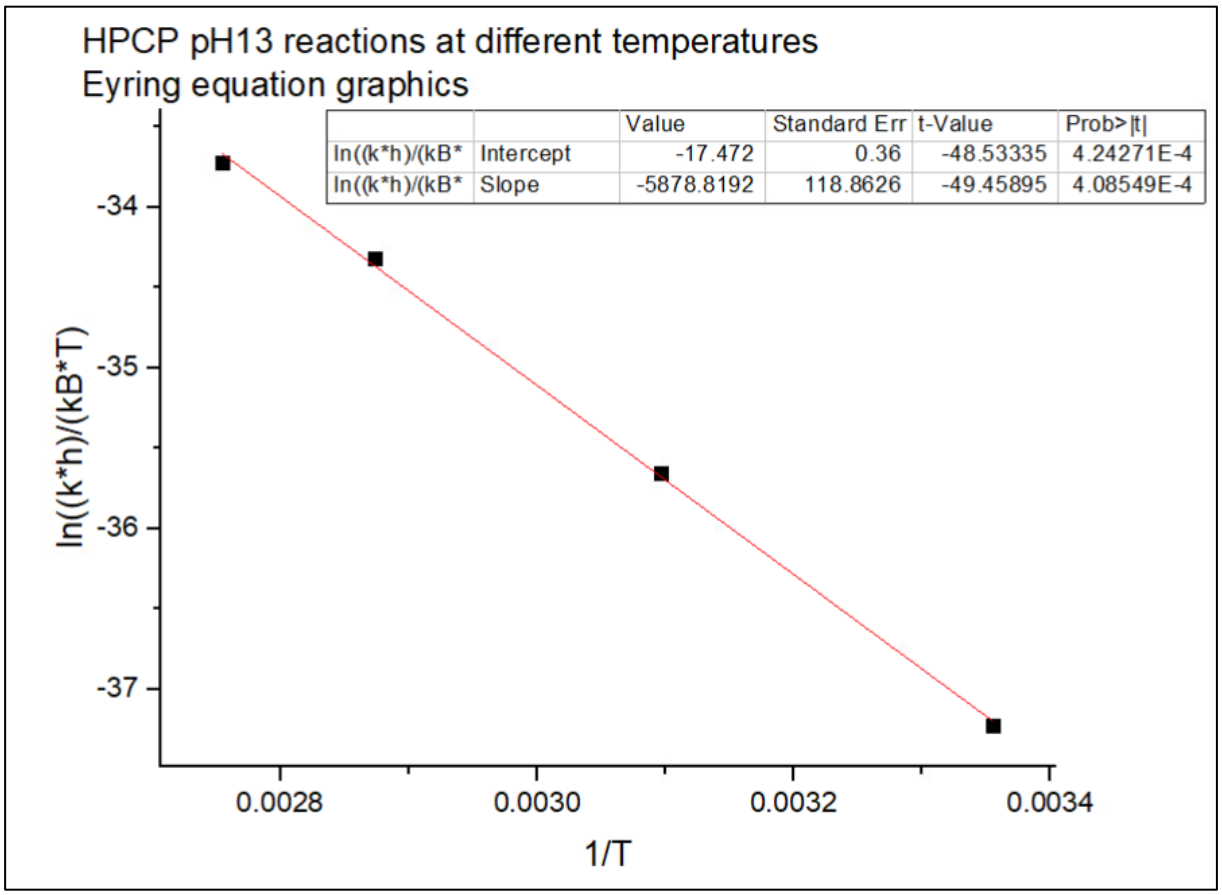

$$y - intercept = \frac{\Delta S^{\neq}}{R} \rightarrow \Delta S^{\neq} = y - intercept * R$$

$$\Delta S^{\neq} = y - intercept * R = -17{,}472 * 8{,}314\ J\ mol^{-1}K^{-1} \approx -145{,}3\ J\ mol^{-1}K^{-1}$$

$$slope = \frac{-\Delta H^{\neq}}{R} \rightarrow \Delta H^{\neq} = -slope * R$$

$$\Delta H^{\neq} = -slope * R = -(-5878{,}8192) * 8{,}314\ J\ mol^{-1}K^{-1} \approx 48{,}88\ kJ/mol$$

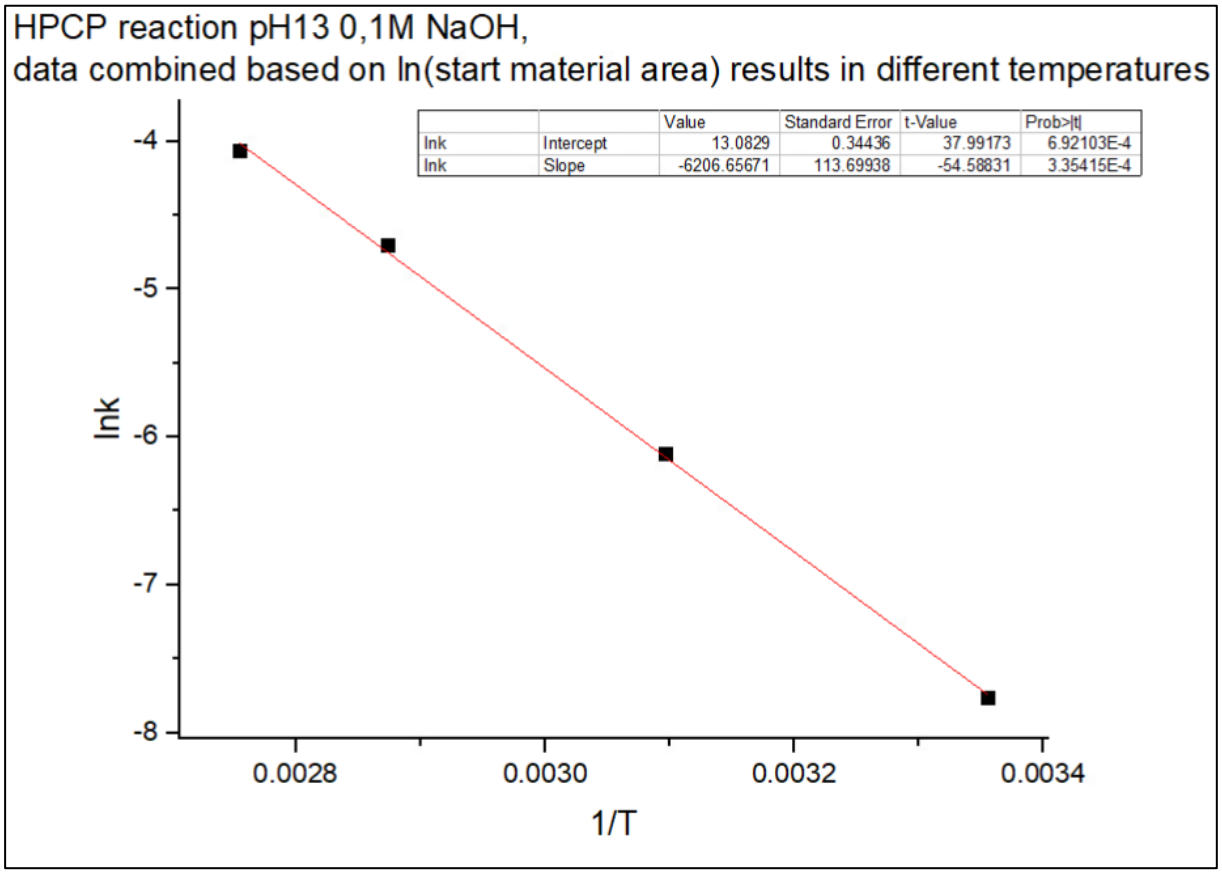

		Value	Standard Error	t-Value	Prob>|t|
lnk	Intercept	13.0829	0.34436	37.99173	6.92103E-4
lnk	Slope	-6206.65671	113.69938	-54.58831	3.35415E-4

$y - intercept = \ln A$

$A = e^{\ln A} = 2{,}718^{13{,}0829} = 480001{,}0206 \approx 4{,}800 * 10^5$

$slope = -\frac{Ea}{R} \rightarrow Ea = -slope * R$

$Ea = -slope * R = -(-6206{,}65671) * 8{,}314\ J\ mol^{-1}K^{-1} \approx 51{,}60\ kJ/mol$

HPCP reaction series for 0.1 M HCl (pH 1) derived from tests conducted in temperatures 25, 50, 75 and 90°C:

	A(X)	B(Y)	C(Y)	D(Y)	E(Y)	F(Y)	G(Y)
Long Name	t/C	k (pH1)	T/K	1/T	h	KB	
Units							
Comments		source area slopes		x-akseli	Planckin vakio	Boltzmanin vakio	y-akseli
F(x)=			273+col(A)	1/col(C)			ln((col(B)*col(E))/((col(F)*col(C))))
1	25	4.44959E-7	298	0.00336	6.6262E-34	1.38E-23	-44.08187
2	50	9.38896E-6	323	0.0031	6.6262E-34	1.38E-23	-41.11312
3	75	1.14687E-4	348	0.00287	6.6262E-34	1.38E-23	-38.68499
4	90	4.5547E-4	363	0.00275	6.6262E-34	1.38E-23	-37.34807

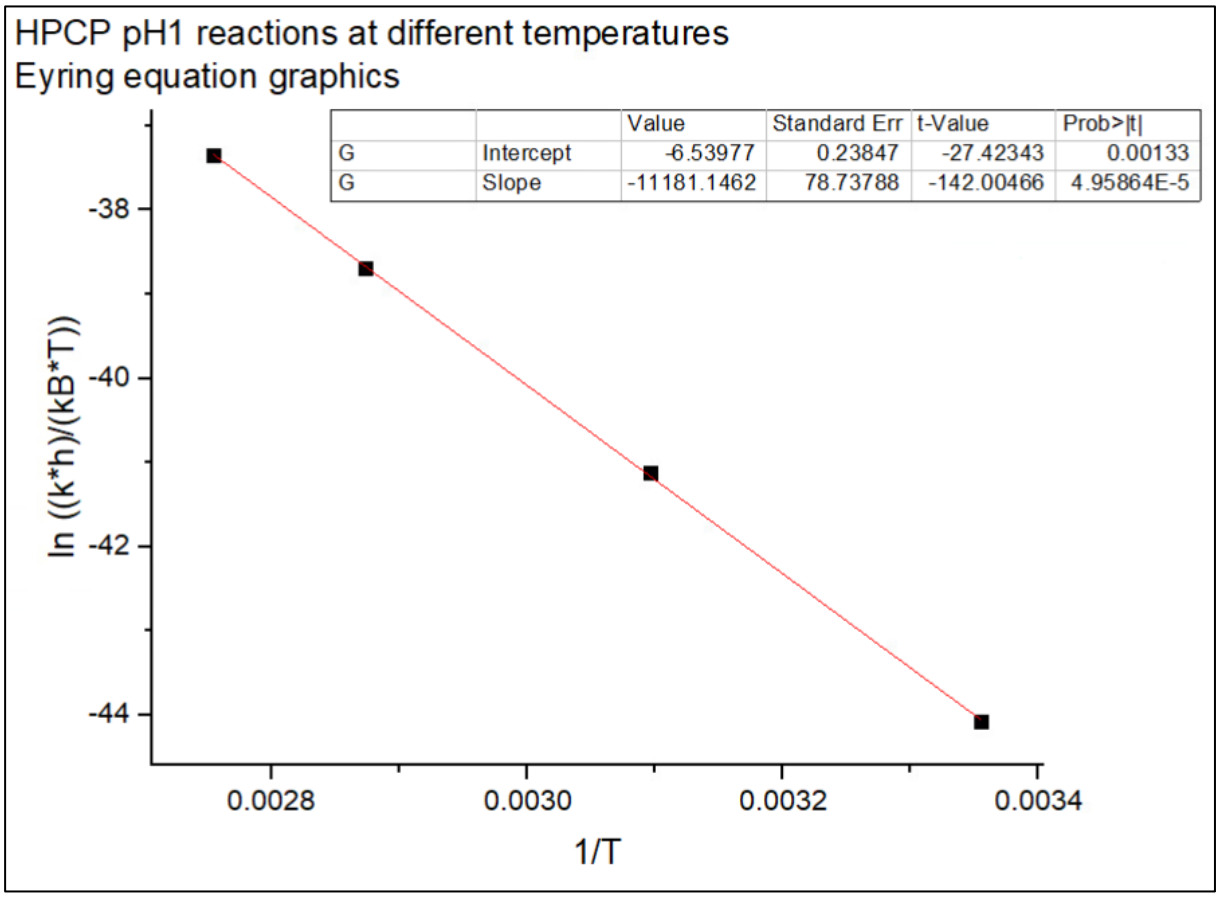

$$y - intercept = \frac{\Delta S^{\neq}}{R} \rightarrow \Delta S^{\neq} = y - intercept * R$$

$$\Delta S^{\neq} = y - intercept * R = -6{,}53977 * 8{,}314\ J\ mol^{-1}K^{-1} \approx -54{,}37\ J\ mol^{-1}K^{-1}$$

$$slope = \frac{-\Delta H^{\neq}}{R} \rightarrow \Delta H^{\neq} = -slope * R$$

$$\Delta H^{\neq} = -slope * R = -(-11181{,}1462) * 8{,}314\ J\ mol^{-1}K^{-1} \approx 92{,}96\ kJ/mol$$

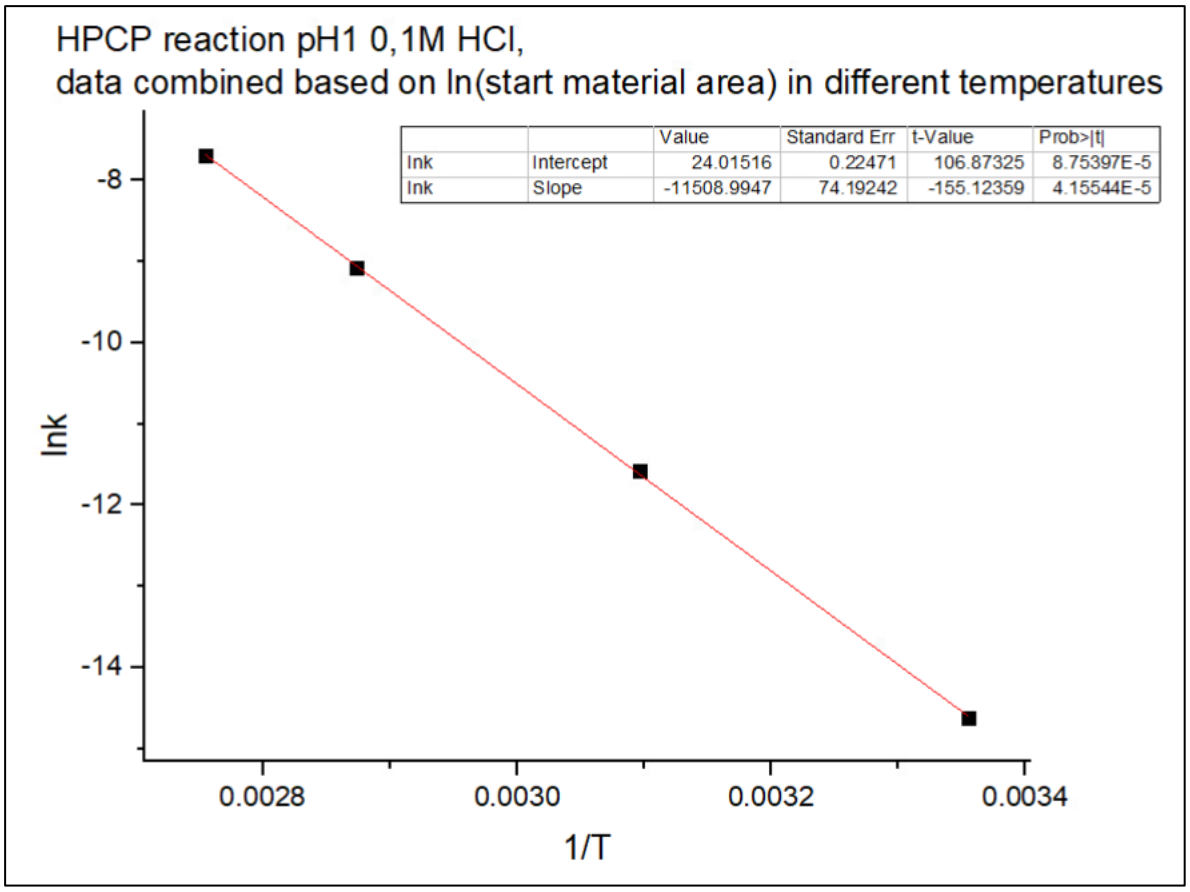

		Value	Standard Err	t-Value	Prob>|t|
lnk	Intercept	24.01516	0.22471	106.87325	8.75397E-5
lnk	Slope	-11508.9947	74.19242	-155.12359	4.15544E-5

$y - intercept = \ln A$

$A = e^{\ln A} = 2{,}718^{24{,}01516} \approx 2{,}683 * 10^{10}$

$slope = -\frac{Ea}{R} \rightarrow Ea = -slope * R$

$Ea = -slope * R = -(-11508{,}9947) * 8{,}314\ J\ mol^{-1}K^{-1} \approx 95{,}69\ kJ/mol$

Appendix 4 Reaction activation parameter calculations for HPNP

HPNP reaction series for 0,025M K_2HPO_4 + 0,005M NaOH + 10,5mM NaCl (pH 10) derived from tests conducted in temperatures 25, 50, 75 and 90°C:

	A(X)	B(Y)	C(Y)	D(Y)	E(Y)	F(Y)	H(Y)
Long Name	t/C	k (pH10)	T/K	1/T	h	KB	ln((k*h)/(kB*T)
Units							
Comments		source area slopes		x-akseli	Planckin vakio	Boltzmanin vakio	y-akseli
F(x)=			273+col(A)	1/col(C)			ln((col(B)*col(E))/((col(F)*col(C))))
1	25	4.74936E-6	298	0.00336	6.6262E-34	1.38E-23	-41.71408
2	50	4.71777E-4	323	0.0031	6.6262E-34	1.38E-23	-37.19614
3	75	0.00281	348	0.00287	6.6262E-34	1.38E-23	-35.48626
4	90	0.00517	363	0.00275	6.6262E-34	1.38E-23	-34.91877

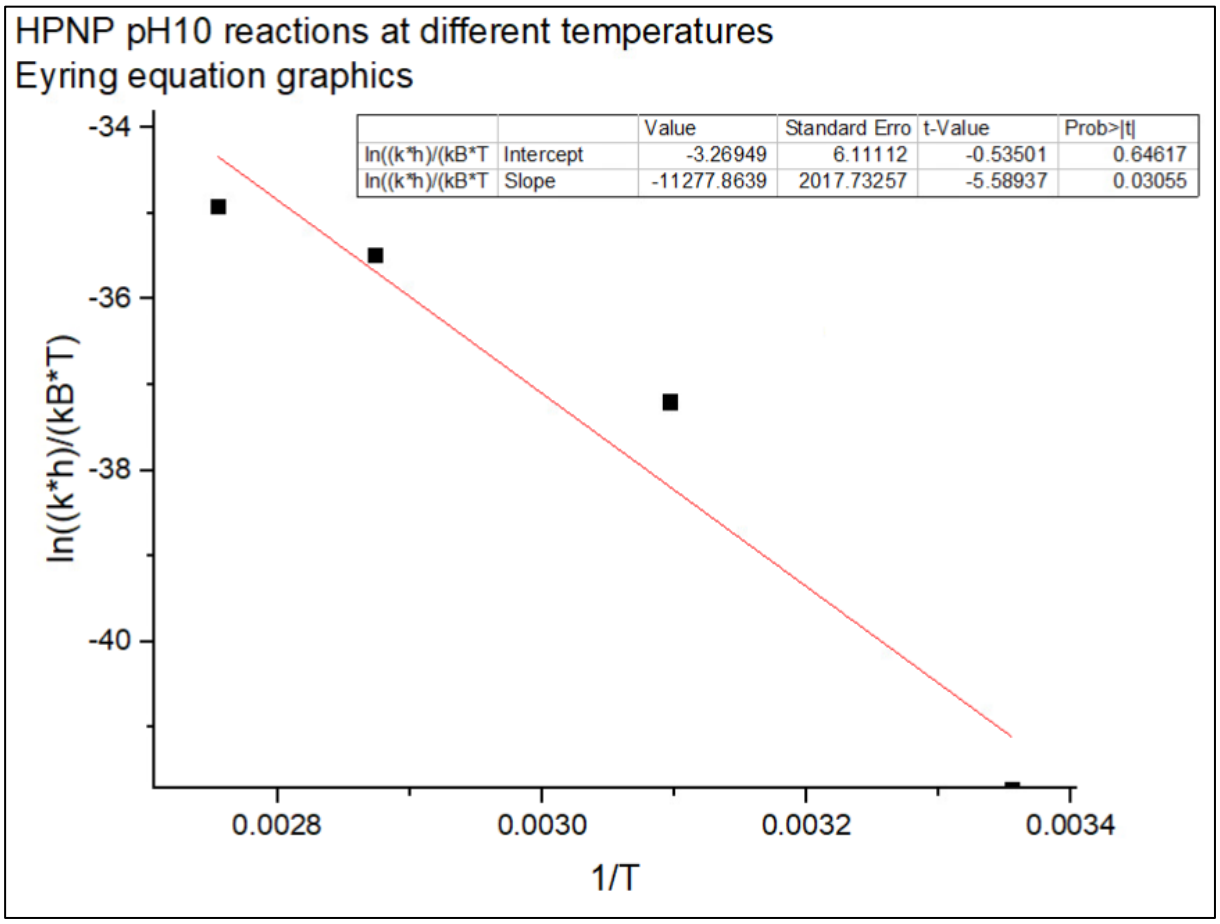

$$y - intercept = \frac{\Delta S^{\neq}}{R} \rightarrow \Delta S^{\neq} = y - intercept * R$$

$$\Delta S^{\neq} = y - intercept * R = -3{,}26949 * 8{,}314\ J\ mol^{-1}K^{-1} \approx -27{,}18\ J\ mol^{-1}K^{-1}$$

$$slope = \frac{-\Delta H^{\neq}}{R} \rightarrow \Delta H^{\neq} = -slope * R$$

$$\Delta H^{\neq} = -slope * R = -(-11277{,}8639) * 8{,}314\ J\ mol^{-1}K^{-1} \approx 93{,}76\ kJ/mol$$

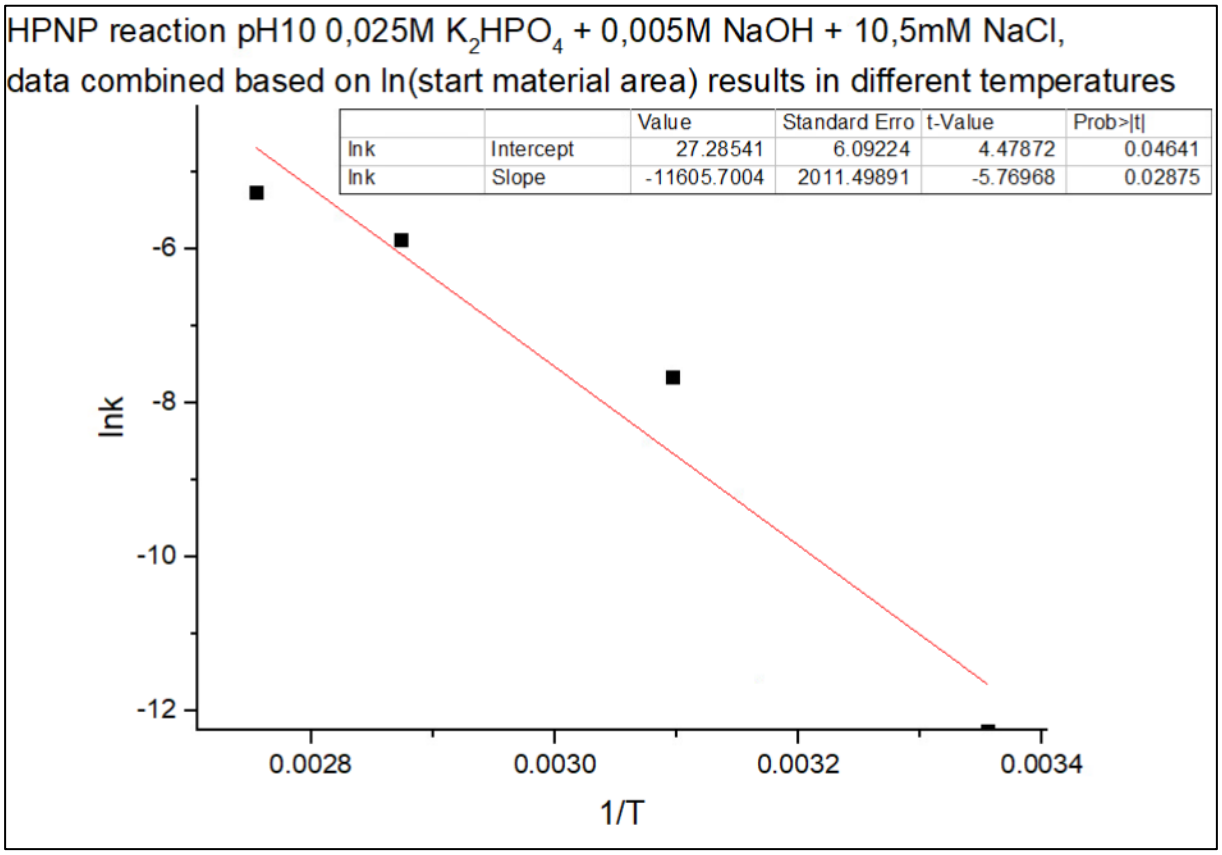

		Value	Standard Erro	t-Value	Prob>|t|
lnk	Intercept	27.28541	6.09224	4.47872	0.04641
lnk	Slope	-11605.7004	2011.49891	-5.76968	0.02875

$y - intercept = \ln A$

$A = e^{\ln A} = 2{,}718^{27{,}28541} \approx 7{,}058 * 10^{11}$

$slope = -\frac{Ea}{R} \rightarrow Ea = -slope * R$

$Ea = -slope * R = -(-11605{,}7004) * 8{,}314\ J\ mol^{-1}K^{-1} \approx 94{,}49\ kJ/mol$

HPNP reaction series for 0.1 M HCl (pH 1) derived from tests conducted in temperatures 25, 50, 75 and 90°C:

	A(X)	B(Y)	C(Y)	D(Y)	E(Y)	F(Y)	G(Y)
Long Name	t/C	k (pH1)	T/K	1/T	h	KB	ln((k*h)/(kB*T)
Units							
Comments		source area slopes		x-akseli	Planckin vakio	Boltzmanin vakio	y-akseli
F(x)=			273+col(A)	1/col(C)			ln((col(B)*col(E))/((col(F)*col(C))))
1	25	5.44575E-4	298	0.00336	6.6262E-34	1.38E-23	-36.97209
2	50	5.92335E-5	323	0.0031	6.6262E-34	1.38E-23	-39.27116
3	75	3.06844E-4	348	0.00287	6.6262E-34	1.38E-23	-37.70086
4	90	0.00201	363	0.00275	6.6262E-34	1.38E-23	-35.86351

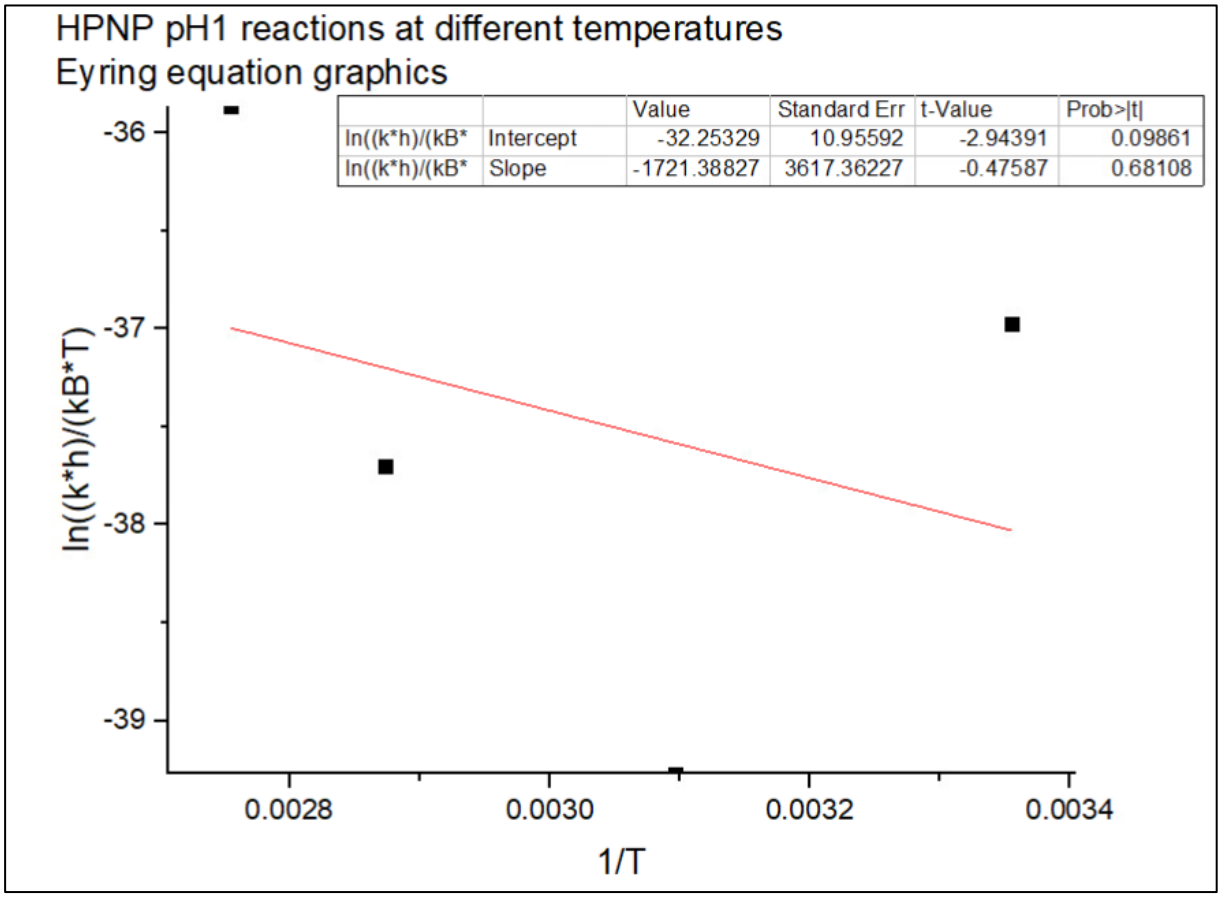

$$y - intercept = \frac{\Delta S^{\neq}}{R} \rightarrow \Delta S^{\neq} = y - intercept * R$$

$$\Delta S^{\neq} = y - intercept * R = -32{,}25329 * 8{,}314\, J\, mol^{-1}K^{-1} \approx -268{,}1\, J\, mol^{-1}K^{-1}$$

$$slope = \frac{-\Delta H^{\neq}}{R} \rightarrow \Delta H^{\neq} = -slope * R$$

$$\Delta H^{\neq} = -slope * R = -(-1721{,}38827) * 8{,}314\, J\, mol^{-1}K^{-1} \approx 14{,}31\, kJ/mol$$

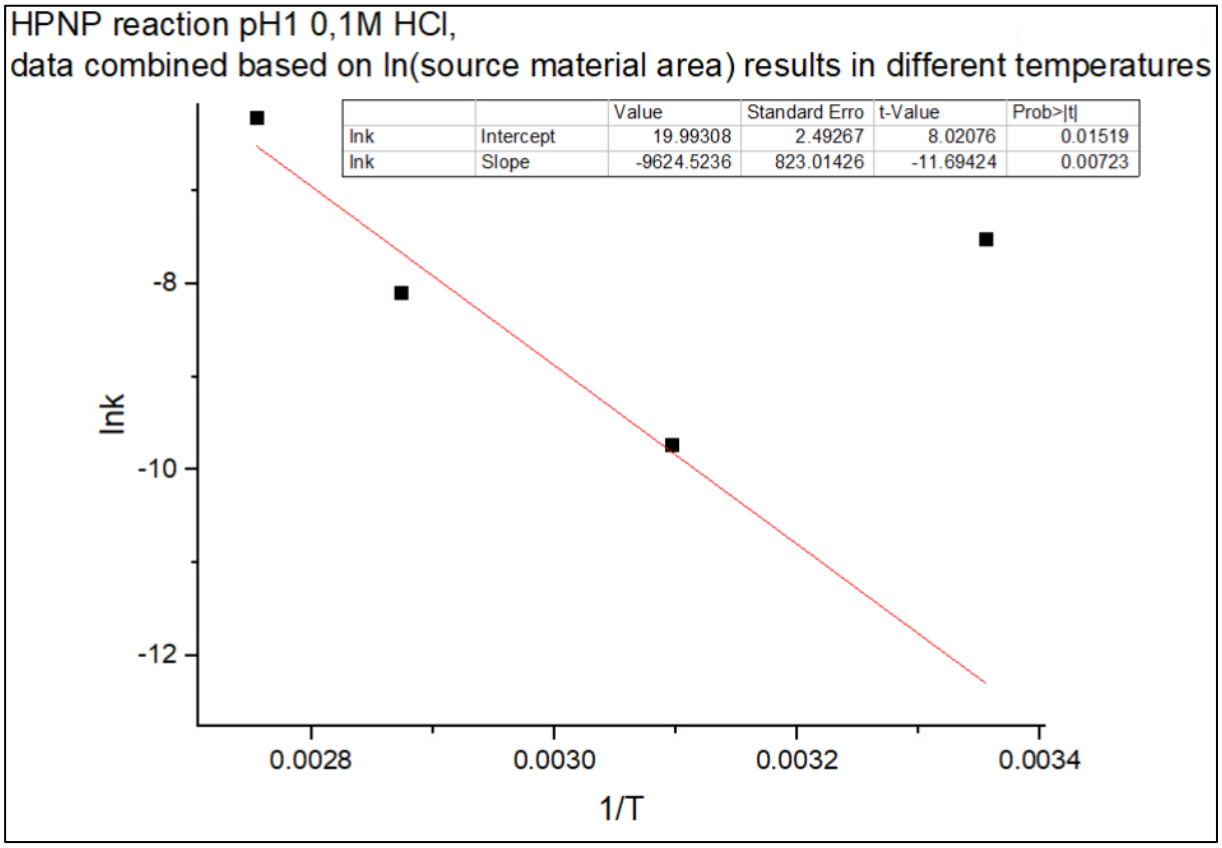

		Value	Standard Erro	t-Value	Prob>|t|
lnk	Intercept	19.99308	2.49267	8.02076	0.01519
lnk	Slope	-9624.5236	823.01426	-11.69424	0.00723

$y - intercept = \ln A$

$A = e^{\ln A} = 2{,}718^{19{,}99308} = 480821680{,}2 \approx 4{,}808 * 10^{8}$

$slope = -\frac{Ea}{R} \rightarrow Ea = -slope * R$

$Ea = -slope * R = -(-9642{,}5236) * 8{,}314\ J\ mol^{-1}K^{-1} \approx 80{,}17\ kJ/mol$